

Structural and Kinetic Study of Reversible CO<sub>2</sub> Fixation by Dicopper Macrocyclic Complexes. From Intramolecular Binding to Self-Assembly of Molecular BoxesAnna Company,<sup>†</sup> Joo-Eun Jee,<sup>§</sup> Xavi Ribas,<sup>†</sup> Josep Maria Lopez-Valbuena,<sup>#,†</sup> Laura Gómez,<sup>†</sup> Montserrat Corbella,<sup>‡</sup> Antoni Llobet,<sup>\*,#||</sup> José Mahía,<sup>⊥</sup> Jordi Benet-Buchholz,<sup>#</sup> Miquel Costas,<sup>\*,†</sup> and Rudi van Eldik<sup>\*,§</sup>

Departament de Química, Universitat de Girona, Campus de Montilivi, E-17071, Girona, Spain, Departament de Química Inorgànica, Universitat de Barcelona, Martí i Franquès, 1-11, E-08028 Barcelona, Spain, Institute of Chemical Research of Catalonia (ICIQ), Avda. Països Catalans 16, E-43007 Tarragona, Spain, Departament de Química, Universitat Autònoma de Barcelona, Cerdanyola del Vallès, E-08193 Barcelona, Spain, Servicios Xerais de Apoio Á Investigación, Universidade da Coruña, E-15071 A Coruña, Spain, and Institute for Inorganic Chemistry, University of Erlangen-Nürnberg, Egerlandstrasse 1, 91058 Erlangen, Germany

Received April 11, 2007

A study of the reversible CO<sub>2</sub> fixation by a series of macrocyclic dicopper complexes is described. The dicopper macrocyclic complexes [Cu<sub>2</sub>(OH)<sub>2</sub>(Me2p)](CF<sub>3</sub>SO<sub>3</sub>)<sub>2</sub>, **1**(CF<sub>3</sub>SO<sub>3</sub>)<sub>2</sub>, and [Cu<sub>2</sub>(μ-OH)<sub>2</sub>(Me2m)](CF<sub>3</sub>SO<sub>3</sub>)<sub>2</sub>, **2**(CF<sub>3</sub>SO<sub>3</sub>)<sub>2</sub>, (Scheme 1) containing terminally bound and bridging hydroxide ligands, respectively, promote reversible inter- and intramolecular CO<sub>2</sub> fixation that results in the formation of the carbonate complexes [{Cu<sub>2</sub>(Me2p)}<sub>2</sub>(μ-CO<sub>3</sub>)](CF<sub>3</sub>SO<sub>3</sub>)<sub>4</sub>, **4**(CF<sub>3</sub>SO<sub>3</sub>)<sub>4</sub>, and [Cu<sub>2</sub>(μ-CO<sub>3</sub>)(Me2m)](CF<sub>3</sub>SO<sub>3</sub>)<sub>2</sub>, **5**(CF<sub>3</sub>SO<sub>3</sub>)<sub>2</sub>. Under a N<sub>2</sub> atmosphere the complexes evolve CO<sub>2</sub> and revert to the starting hydroxo complexes **1**(CF<sub>3</sub>SO<sub>3</sub>)<sub>2</sub> and **2**(CF<sub>3</sub>SO<sub>3</sub>)<sub>2</sub>, a reaction the rate of which linearly depends on [H<sub>2</sub>O]. In the presence of water, attempts to crystallize **5**(CF<sub>3</sub>SO<sub>3</sub>)<sub>2</sub> afford [{Cu<sub>2</sub>(Me2m)(H<sub>2</sub>O)}<sub>2</sub>(μ-CO<sub>3</sub>)](CF<sub>3</sub>SO<sub>3</sub>)<sub>4</sub>, **6**(CF<sub>3</sub>SO<sub>3</sub>)<sub>4</sub>, which appears to rapidly convert to **5**(CF<sub>3</sub>SO<sub>3</sub>)<sub>2</sub> in acetonitrile solution. [Cu<sub>2</sub>(OH)<sub>2</sub>(H3m)]<sup>2+</sup>, **7**, which contains a larger macrocyclic ligand, irreversibly reacts with atmospheric CO<sub>2</sub> to generate cage-like [{Cu<sub>2</sub>(H3m)}<sub>2</sub>(μ-CO<sub>3</sub>)](ClO<sub>4</sub>)<sub>4</sub>, **8**(ClO<sub>4</sub>)<sub>4</sub>. However, addition of 1 equiv of HClO<sub>4</sub> per Cu generates [Cu<sub>2</sub>(H3m)(CH<sub>3</sub>CN)<sub>4</sub>]<sup>4+</sup> (**3**), and subsequent addition of Et<sub>3</sub>N under air reassembles **8**. The carbonate complexes **4**(CF<sub>3</sub>SO<sub>3</sub>)<sub>4</sub>, **5**(CF<sub>3</sub>SO<sub>3</sub>)<sub>2</sub>, **6**(CF<sub>3</sub>SO<sub>3</sub>)<sub>4</sub>, and **8**(ClO<sub>4</sub>)<sub>4</sub> have been characterized in the solid state by X-ray crystallography. This analysis reveals that **4**(CF<sub>3</sub>SO<sub>3</sub>)<sub>4</sub>, **6**(CF<sub>3</sub>SO<sub>3</sub>)<sub>4</sub>, and **8**(ClO<sub>4</sub>)<sub>4</sub> consist of self-assembled molecular boxes containing two macrocyclic dicopper complexes, bridged by CO<sub>3</sub><sup>2-</sup> ligands. The bridging mode of the carbonate ligand is *anti-anti-μ-η<sup>1</sup>:η<sup>1</sup>* in **4**(CF<sub>3</sub>SO<sub>3</sub>)<sub>4</sub>, *anti-anti-μ-η<sup>2</sup>:η<sup>1</sup>* in **6**(CF<sub>3</sub>SO<sub>3</sub>)<sub>4</sub> and *anti-anti-μ-η<sup>2</sup>:η<sup>2</sup>* in **5**(CF<sub>3</sub>SO<sub>3</sub>)<sub>2</sub> and **8**(ClO<sub>4</sub>)<sub>4</sub>. Magnetic susceptibility measurements on **4**(CF<sub>3</sub>SO<sub>3</sub>)<sub>4</sub>, **6**(CF<sub>3</sub>SO<sub>3</sub>)<sub>4</sub>, and **8**(ClO<sub>4</sub>)<sub>4</sub> indicate that the carbonate ligands mediate antiferromagnetic coupling between each pair of bridged Cu<sup>II</sup> ions ( $J = -23.1, -108.3, \text{ and } -163.4 \text{ cm}^{-1}$ , respectively,  $H = -JS_1S_2$ ). Detailed kinetic analyses of the reaction between carbon dioxide and the macrocyclic complexes **1**(CF<sub>3</sub>SO<sub>3</sub>)<sub>2</sub> and **2**(CF<sub>3</sub>SO<sub>3</sub>)<sub>2</sub> suggest that it is actually hydrogen carbonate formed in aqueous solution on dissolving CO<sub>2</sub> that is responsible for the observed formation of the different carbonate complexes controlled by the binding mode of the hydroxy ligands. This study shows that CO<sub>2</sub> fixation can be used as an on/off switch for the reversible self-assembly of supramolecular structures based on macrocyclic dicopper complexes.

## Introduction

Fixation of CO<sub>2</sub> mediated by transition metal complexes is a reaction of biological relevance, and it has potential

environmental and technological implications.<sup>1,2</sup> Several copper(II) complexes are well-known to perform this reaction, usually resulting in the formation of carbonate complexes,<sup>3–5</sup> and a carbamate-bridged Cu<sup>II</sup> species has

\* To whom correspondence should be addressed. E-mail: miquel.costas@udg.edu (M.C.); vaneldik@chemie.uni-erlangen.de (R.v.E.); allobet@icq.es (A.L.).

<sup>†</sup> Universitat de Girona.

<sup>‡</sup> Universitat de Barcelona.

<sup>#</sup> Institute of Chemical Research of Catalonia.

<sup>⊥</sup> Universidade da Coruña.

<sup>§</sup> University of Erlangen-Nürnberg.

<sup>||</sup> Universitat Autònoma de Barcelona.

(1) Yin, X.; Moss, J. R. *Coord. Chem. Rev.* **1999**, *181*, 27–59 and references therein.

(2) Parson, E. A.; Keith, D. W. *Science* **1998**, *282*, 1053–1054.

(3) Escuer, A.; Mautner, F. A.; Peñalba, E.; Vicente, R. *Inorg. Chem.* **1998**, *37*, 4190–4196.

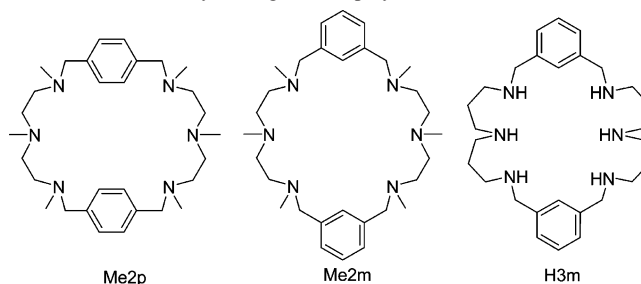
(4) Mao, Z.-W.; Heinemann, F. W.; Liehr, G.; van Eldik, R. *J. Chem. Soc. Dalton Trans* **2001**, *24*, 3652–3662 and references therein.

been recently reported.<sup>6</sup> Reversible CO<sub>2</sub> fixation has also been documented, and more recently, this process has found use in CO<sub>2</sub> separation and purification from air.<sup>7</sup> Surprisingly, details of the reaction mechanism by which copper complexes fixate CO<sub>2</sub> have been seldom studied, but by analogy to detailed studies on Zn(II) catalyzed hydration processes,<sup>8–11</sup> such reactions are expected to occur via nucleophilic attack of coordinated water or hydroxide on CO<sub>2</sub>.<sup>12–14</sup>

On the other hand, crown ethers and related aza-analogous macrocycles constitute highly preorganized cavities with the ability to selectively interact with cationic, neutral, or anionic substrates.<sup>15–19</sup> This type of macrocyclic ligands provides excellent bimetallic scaffolds which give control over the metal–metal distance and its relative orientation as a way to modulate intermetallic interactions. This control has previously found application in promoting interesting properties such as electronic delocalization over two metal sites,<sup>20,21</sup> cooperative effects in catalysis,<sup>22,23</sup> and small molecule binding and/or activation.<sup>24–26</sup> CO<sub>2</sub> fixation by dimetallic macrocyclic complexes rarely occurs intermolecularly, and intramolecular reactions give rise to carbonate or bicarbonate bridging ligands buried within the hydrophobic macrocyclic cavity.<sup>6,26,27</sup>

We have recently described the preparation and structural characterization of isomerically related macrocyclic hydroxo-containing dicopper complexes [Cu<sub>2</sub>(OH)<sub>2</sub>(Me2p)](CF<sub>3</sub>SO<sub>3</sub>)<sub>2</sub>, **1**(CF<sub>3</sub>SO<sub>3</sub>)<sub>2</sub>, and [Cu<sub>2</sub>(μ-OH)<sub>2</sub>(Me2m)](CF<sub>3</sub>SO<sub>3</sub>)<sub>2</sub>, **2**(CF<sub>3</sub>SO<sub>3</sub>)<sub>2</sub>.

**Scheme 1.** Macrocylic Ligands Employed in This Work



SO<sub>3</sub>)<sub>2</sub>.<sup>28</sup> While the latter contains the rather common Cu<sub>2</sub>(μ-OH)<sub>2</sub> unit, the former is a rare example because it contains two copper atoms, each having a terminally bound hydroxide ligand. **1**(CF<sub>3</sub>SO<sub>3</sub>)<sub>2</sub> and **2**(CF<sub>3</sub>SO<sub>3</sub>)<sub>2</sub> constitute a unique platform to study the CO<sub>2</sub> fixation reaction on well-defined copper–hydroxide complexes described herein. In addition, the present study explores the use of reversible CO<sub>2</sub> fixation as a novel suitable chemical switch for the reversible self-assembly of the dicopper macrocyclic complexes **1**(CF<sub>3</sub>SO<sub>3</sub>)<sub>2</sub>, **2**(CF<sub>3</sub>SO<sub>3</sub>)<sub>2</sub>, and [Cu<sub>2</sub>(H3m)(CH<sub>3</sub>CN)<sub>4</sub>](ClO<sub>4</sub>)<sub>4</sub>, **3**(ClO<sub>4</sub>)<sub>4</sub> (Scheme 1) into higher-order supramolecular structures.

## Experimental Section

**Materials and Synthesis.** Solvents were purchased from SDS as reagent grade. Acetonitrile (ACN) was distilled over CaH<sub>2</sub> and stored over molecular sieves. Diethyl ether was distilled over Na/benzophenone under nitrogen. Acetone was dried over CaCl<sub>2</sub> and stored over molecular sieves. Unless noted otherwise, all reagents were purchased from commercial sources and used as received. Preparation and handling of air-sensitive materials were carried out under argon or N<sub>2</sub> atmosphere using standard Schlenk techniques. CO<sub>2</sub> gas was obtained from Abelló-Linde.

**Preparation of the Complexes.** *Caution: Perchlorate salts are potentially explosive and should be handled with care!*

**Ligand Synthesis.** 3,6,9,16,19,22-Hexamethyl-3,6,9,16,19,22-hexaazatricyclo[22.2.2.2<sup>11,14</sup>]triaconta-1(26),11(12),13,24,27,29-hexaene, Me2p, 3,6,9,17,20,23-hexamethyl-3,6,9,17,20,23-hexaazatricyclo[23.3.1.1<sup>11,15</sup>]triaconta-1(29),11(30),12,14,25,27-hexaene, Me2m, and 3,7,11,19,23,27-hexaazatricyclo[27.3.1.1<sup>13,17</sup>]tetraatriaconta-1(32),13,15,17(34),29(33),30-hexaene, H3m, were prepared as previously reported in the literature.<sup>29–32</sup>

**Complex Synthesis.** **1**(CF<sub>3</sub>SO<sub>3</sub>)<sub>2</sub> and **2**(CF<sub>3</sub>SO<sub>3</sub>)<sub>2</sub> were prepared as previously reported.<sup>28</sup>

[Cu<sub>2</sub>(H3m)(CH<sub>3</sub>CN)<sub>4</sub>](ClO<sub>4</sub>)<sub>4</sub>·3/2H<sub>2</sub>O, [3(ClO<sub>4</sub>)<sub>4</sub>]<sub>3</sub>·2H<sub>2</sub>O. Ligand H3m (0.046 g, 0.099 mmol) and Cu(ClO<sub>4</sub>)<sub>2</sub>·6H<sub>2</sub>O (0.073 g, 0.2 mmol) were dissolved in 3 mL of anhydrous CH<sub>3</sub>CN and degassed with Ar. Stirring under Ar for 24 h and slow diffusion of diethyl ether allowed the formation of blue-violet crystals in 82% yield (0.093 g, 0.081 mmol). FT-IR (ATR): ν = 3217, 2251, 1462, 1439, 1144, 1113, 1088, and 629 cm<sup>-1</sup>. Anal. (%) Calcd for

- (5) Palmer, D. A.; van Eldik, R. *Chem. Rev.* **1983**, *83*, 651–731.
- (6) Garcia-Espana, E.; Gavina, P.; Latorre, J.; Soriano, C.; Verdejo, B. *J. Am. Chem. Soc.* **2004**, *126*, 5082–5083.
- (7) Appel, A. M.; Newell, R.; DuBois, D. L.; Rakowski DuBois, M. *Inorg. Chem.* **2005**, *44*, 3046–3056.
- (8) Parkin, G. *Chem. Rev.* **2004**, *104*, 699–768.
- (9) Kimura, E. *Acc. Chem. Res.* **2001**, *34*, 171–179.
- (10) Hartmann, M.; Clark, T.; van Eldik, R. *J. Am. Chem. Soc.* **1997**, *119*, 7843–7850.
- (11) Sola, M.; Lledos, A.; Duran, M.; Bertran, J. *J. Am. Chem. Soc.* **1992**, *114*, 869–877.
- (12) Bazzicalupi, C.; Bencini, A.; Bencini, A.; Bianchi, A.; Corana, F.; Fusi, V.; Giorgi, C.; Paoli, P.; Paoletti, P.; Valtancoli, B.; Zanchini, C. *Inorg. Chem.* **1996**, *35*, 5540–5548.
- (13) Kitajima, N.; Hikichi, S.; Tanaka, M.; Morooka, Y. *J. Am. Chem. Soc.* **1993**, *115*, 5496–5508.
- (14) Leitner, W. *Coord. Chem. Rev.* **1996**, *153*, 257–284.
- (15) Lindoy, L. F. *The Chemistry of Macrocyclic Ligand Complexes*; Cambridge University Press: Cambridge, 1992.
- (16) Izatt, R. M.; Pawlak, K.; Bradshaw, J. S.; Bruening, R. L. *Chem. Rev.* **1995**, *95*, 2529–2586.
- (17) Alexander, V. *Chem. Rev.* **1995**, *95*, 273–342.
- (18) Anda, C.; Llobet, A.; Martell, A. E.; Riebenspies, J.; Berni, E.; Solans, X. *Inorg. Chem.* **2004**, *43*, 2793–2802.
- (19) Anda, C.; Martínez, M.-A.; Llobet, A. *Supramol. Chem.* **2005**, *17*, 257–266.
- (20) Farrar, J. A.; Grinter, R.; Neese, F.; Nelson, J.; Thomson, A. J. *J. Chem. Soc. Dalton Trans.* **1997**, 4083–4087.
- (21) Harding, C.; Nelson, J.; Symons, M. C. R.; Wyatt, J. *J. Chem. Soc. Chem. Comm.* **1994**, 2499–2500.
- (22) Lu, T.; Zhuang, X.; Li, Y.; Chen, S. *J. Am. Chem. Soc.* **2004**, *126*, 4760–4761.
- (23) Bencini, A.; Berni, E.; Bianchi, A.; Fedi, V.; Giorgi, C.; Paoletti, P.; Valtancoli, B. *Inorg. Chem.* **1999**, *38*, 6323–6325.
- (24) Menif, R.; Martell, A. E. *J. Chem. Soc. Chem. Commun.* **1989**, 1521–1523.
- (25) Bol, J. E.; Driessen, W. L.; Ho, R. Y. N.; Maase, B.; Que, L., Jr.; Reedijk, J. *Angew. Chem., Int. Ed.* **1997**, *36*, 998–1000.
- (26) Kersting, B. *Angew. Chem., Int. Ed.* **2001**, *40*, 3987–3990.
- (27) Dussart, Y.; Harding, C.; Dalggaard, P.; MacKenzie, C.; Kadirvelraj, R.; MacKee, V.; Nelson, J. *J. Chem. Soc. Dalton Trans* **2002**, 1704–1713.

- (28) Costas, M.; Ribas, X.; Poater, A.; Lopez-Valbuena, J. M.; Xifra, R.; Company, A.; Duran, M.; Sola, M.; Llobet, A.; Corbella, M.; Uson, M. A.; Mahia, J.; Solans, X.; Shan, X.; Benet-Buchholz, J. *Inorg. Chem.* **2006**, *45*, 3569–3581.
- (29) Menif, R.; Martell, A. E.; Squattrito, P. J.; Clearfield, A. *Inorg. Chem.* **1990**, *29*, 4723–4729.
- (30) Pietraszkiewicz, M.; Gasiorowski, R. *Chem. Ber.* **1990**, *123*, 405–406.
- (31) Llobet, A.; Riebenspies, J.; Martell, A. E. *Inorg. Chem.* **1994**, *33*, 5946–51.
- (32) Clifford, T.; Danby, A. M.; Lightfoot, P.; Richens, D. T.; Hay, R. W. *J. Chem. Soc. Dalton Trans.* **2001**, 240–246.

$\text{Cu}_2\text{C}_{36}\text{H}_{58}\text{N}_{10}\text{O}_{16}\text{Cl}_4 \cdot 3/2\text{H}_2\text{O}$ : C 36.56, H 5.20, N 11.84. Found: C 36.51, H 5.46, N 12.08. UV-vis ( $\text{CH}_3\text{CN}$ ),  $\lambda_{\text{max}}$  ( $\epsilon$ ): 656 nm ( $490 \text{ M}^{-1} \text{ cm}^{-1}$ ).

$\{[\text{Cu}_2(\text{Me2p})_2(\mu\text{-CO}_3)_2](\text{CF}_3\text{SO}_3)_4 \cdot 8\text{H}_2\text{O}, [4(\text{CF}_3\text{SO}_3)_4] \cdot 8\text{H}_2\text{O}$ .

**Method A.**  $1(\text{CF}_3\text{SO}_3)_2$  (25 mg, 0.025 mmol) was dissolved in ACN (2 mL) to give a blue-gray solution. The mixture was stirred under a  $\text{CO}_2$  atmosphere for 4 h, and then the solution was filtered through Celite. Ether diffusion over this solution under a  $\text{CO}_2$  atmosphere afforded the product as highly moisture-sensitive violet blocks.

**Method B.** Me2p (50.6 mg, 0.10 mmol) and  $\text{Cu}(\text{CF}_3\text{SO}_3)_2$  (72 mg, 0.20 mmol) were charged in a 10 mL flask and dissolved in  $\text{CH}_3\text{CN}/\text{H}_2\text{O}$  20:1 (2 mL) to form a deep purple solution. The mixture was stirred for 30 min, and then  $\text{Na}_2\text{CO}_3$  (10.7 mg, 0.11 mmol) was added directly as a solid while keeping the mixture under vigorous agitation.  $\text{Na}_2\text{CO}_3$  got dissolved gradually to give a dark blue-violet solution. The mixture was stirred for 20 h and then filtered through Celite. Ether diffusion over this solution afforded after 3 days large violet blocks. The solvent was decanted and the crystalline solid dried under vacuum (95 mg, 93%). FT-IR (ATR):  $\nu = 3495, 1543, 1474, 1335, 1248, 1160, 1029$ , and  $636 \text{ cm}^{-1}$ . Anal. (%) Calcd for  $\text{C}_{66}\text{H}_{100}\text{N}_{12}\text{Cu}_4\text{O}_{18}\text{F}_{12}\text{S}_4 \cdot 8\text{H}_2\text{O}$ : C 37.67, N 7.99, H 5.56, S 6.10. Found: C 37.41, N 7.77, H 5.71, S 6.04. UV-vis ( $\text{CH}_3\text{CN}$ ):  $\lambda_{\text{max}}$  ( $\epsilon$ ) = 209 (5490), 285 (2250), 504 (645), 641 nm ( $680 \text{ M}^{-1} \text{ cm}^{-1}$ ). ESI-MS ( $m/z$ ): 831  $[\text{4} \cdot (\text{CF}_3\text{SO}_3)_2]^{2+}$ .

$[\text{Cu}_2(\mu\text{-CO}_3)(\text{Me2m})](\text{CF}_3\text{SO}_3)_2 \cdot 1/2\text{CH}_2\text{Cl}_2 \cdot 2\text{H}_2\text{O}, [5(\text{CF}_3\text{SO}_3)_2] \cdot 1/2\text{CH}_2\text{Cl}_2 \cdot 2\text{H}_2\text{O}$ .  $2(\text{CF}_3\text{SO}_3)_2$  (25 mg, 0.025 mmol) was dissolved in dry dichloromethane (2 mL) to give a blue solution. The mixture was stirred under a  $\text{CO}_2$  atmosphere for 4 h to give a bright green solution which was filtered through Celite. Ether diffusion over this solution afforded olive-green blocks mixed with blue crystals corresponding to  $6(\text{CF}_3\text{SO}_3)_2$ . Olive-green blocks were picked up manually. FT-IR (ATR):  $\nu = 3504, 1491, 1458, 1388, 1250, 1158, 1026$ , and  $635 \text{ cm}^{-1}$ . Anal. (%) Calcd for  $\text{C}_{33}\text{H}_{50}\text{N}_6\text{Cu}_2\text{O}_9\text{F}_6\text{S}_2 \cdot 1/2\text{CH}_2\text{Cl}_2 \cdot 2\text{H}_2\text{O}$ : C 38.01, N 7.94, H 5.24, S 6.06. Found: C 38.17, N 8.16, H 5.51, S 5.58. UV-vis ( $\text{CH}_3\text{CN}$ ):  $\lambda_{\text{max}}$  ( $\epsilon$ ) = 287 (9000), 381 (3200), 663 (610), 798 nm ( $930 \text{ M}^{-1} \text{ cm}^{-1}$ ). ESI-MS ( $m/z$ ): 831  $[\text{5} \cdot (\text{CF}_3\text{SO}_3)]^+$ .

$\{[\text{Cu}_2(\text{Me2m})(\text{H}_2\text{O})_2(\mu\text{-CO}_3)_2](\text{CF}_3\text{SO}_3)_4 \cdot 4\text{H}_2\text{O}, [6(\text{CF}_3\text{SO}_3)_4] \cdot 4\text{H}_2\text{O}$ . Me2m (50.3 mg, 0.10 mmol) and  $\text{Cu}(\text{CF}_3\text{SO}_3)_2$  (75 mg, 0.20 mmol) were charged in a 10 mL flask and dissolved in  $\text{CH}_3\text{CN}/\text{H}_2\text{O}$  20:1 (2 mL) to form a deep blue solution. The mixture was stirred for 30 min, and then  $\text{Na}_2\text{CO}_3$  (10.7 mg, 0.11 mmol) was added directly as a solid while keeping the mixture under vigorous agitation.  $\text{Na}_2\text{CO}_3$  gradually dissolved to give a dark blue-green solution. The mixture was stirred for 15 h under a  $\text{CO}_2$  atmosphere and then filtered through Celite. Ether diffusion over this solution afforded after 4 days large blue blocks. The solvent was decanted and the crystalline solid dried under vacuum (67 mg, 64%). FT-IR (ATR):  $\nu = 3505, 1491, 1458, 1387, 1248, 1159, 1026$ , and  $635 \text{ cm}^{-1}$ . Anal. (%) Calcd for  $\text{C}_{66}\text{H}_{102}\text{N}_{12}\text{Cu}_4\text{O}_{20}\text{F}_{12}\text{S}_4 \cdot 4\text{H}_2\text{O}$ : C 38.33, N 8.13, H 5.46, S 6.20. Found: C 38.17, N 8.16, H 5.51, S 5.58. UV-vis ( $\text{CH}_3\text{CN}$ ):  $\lambda_{\text{max}} = 293, 710 \text{ nm}$ . ESI-MS ( $m/z$ ): 831  $[\text{5} \cdot (\text{CF}_3\text{SO}_3)]^+$ .

$\{[\text{Cu}_2(\text{H3m})_2(\mu\text{-CO}_3)_2](\text{ClO}_4)_4 \cdot 6\text{H}_2\text{O} \cdot \text{CH}_3\text{COCH}_3, [8(\text{ClO}_4)_4] \cdot 6\text{H}_2\text{O} \cdot \text{CH}_3\text{COCH}_3$ . H3m (0.035 g, 0.075 mmol) and  $\text{Cu}(\text{ClO}_4)_2 \cdot 6\text{H}_2\text{O}$  (0.054 g, 0.15 mmol) were dissolved in  $\text{CH}_2\text{Cl}_2/\text{CH}_3\text{OH}$  20:80 (3 mL). An Ar-purged solution of 0.5 mM NaOH (0.3 mL, 0.15 mmol) was added, and the mixture was stirred for 10 min. The resulting solution was filtered and exposed to open air overnight. Blue crystals were deposited (0.065 g, 0.035 mmol, 94%). FT-IR (ATR):  $\nu = 3245, 1486, 1452, 1117$  and  $671 \text{ cm}^{-1}$ . Anal. Calcd for  $\text{Cu}_4\text{C}_{58}\text{H}_{92}\text{N}_{12}\text{O}_{22}\text{Cl}_4 \cdot 6\text{H}_2\text{O} \cdot \text{CH}_3\text{COCH}_3$ : C 39.15, H 5.92, N 8.98. Found: C 38.77, H 5.50, N 8.76; UV-vis ( $\text{CH}_3\text{CN}$ ):  $\lambda_{\text{max}}$

( $\epsilon$ ) = 266 (14 700), 370 (sh, 2570), 676 nm ( $1310 \text{ M}^{-1} \text{ cm}^{-1}$ ). ESI-MS ( $m/z$ ): 1605  $[\text{8} \cdot (\text{ClO}_4)_3]^+$ .

**Physical Methods.** FT-IR spectra were recorded on a Mattson-Galaxy Satellite FT-IR spectrophotometer containing a MKII Golden Gate Single Reflection ATR System. Elemental analyses were conducted in a Carlo Erba Instrument, Mod. CHNS 1108. UV-vis spectroscopy was performed on a Cary 50 Scan (Varian) UV-vis spectrophotometer with 1 cm quartz cells. Variable-temperature magnetic susceptibility measurements were carried out on polycrystalline samples with a Quantum Design MPMS-XL SQUID susceptometer (**4** and **6**) and on a Faraday-type magnetometer (MANIC DSM8) equipped with a Bruker BE15 electromagnet and an Oxford CF 1200S cryogenic apparatus **8** between 2 and 300 K, at the "Servei de Magnetoquímica" (Universitat de Barcelona). The diamagnetic corrections were evaluated from Pascal's constants. The fit was performed by minimizing the function  $R = \sum(\chi_M \cdot T_{\text{expt}} - \chi_M \cdot T_{\text{calcd}})^2 / \sum(\chi_M \cdot T_{\text{expt}})$ .<sup>2</sup>

**Crystallographic Studies.** Single-crystal X-ray analyses were performed on a Bruker Smart CCD (**4–6**) and a Siemens CCD (**3** and **8**) diffractometers using Mo  $K\alpha$  radiation ( $\lambda = 0.71073 \text{ \AA}$ ). The data collection was executed using the SMART program. Absorption corrections were carried out using SADABS. Cell refinements and data reduction were made by the SAINT program. The structures were determined by direct methods using the SHELXTL program and refined using full-matrix least-squares. All non-hydrogen atoms were refined anisotropically, whereas the hydrogen atoms were placed at the calculated positions and included in the final stage of refinements with fixed thermal and positional parameters. The crystallographic refinement parameters for the complexes are summarized in Table 1, and the selected bond distances and angles are listed in Table 2 and Table S1 (Supporting Information).

The crystals used for structure determination contain in most of the cases solvent molecules, which make their manipulation extremely difficult, and have also disordered anions. Due to these difficulties, some of the data sets are complicated to collect and not of the best quality for refinement.

**Kinetic Measurements.** UV-vis spectra were recorded in gastight cuvettes on a Shimadzu UV-2100 spectrophotometer equipped with a thermostated ( $\pm 0.1 \text{ }^\circ\text{C}$ ) cell compartment. The saturated  $\text{CO}_2$  solution was prepared by purging the solution with  $\text{CO}_2$  at a rate of 1 mL/min. In a typical experiment, a solution was mixed in varying volume ratios with a saturated  $\text{CO}_2$  solution in a gastight syringe to obtain the relative  $\text{CO}_2$  concentration. The concentration of dissolved  $\text{CO}_2$  in different water-ACN mixtures was determined by a pH titration following saturation of the solvent with  $\text{CO}_2(\text{g})$  at  $25 \text{ }^\circ\text{C}$  and atmospheric pressure. In the case of pure ACN, a saturated  $\text{CO}_2$  solution was diluted (1:4) with water in order to perform the pH titration. The observed rate constants were measured by conventional UV-vis spectrophotometry. The kinetics of the reaction of  $1(\text{CF}_3\text{SO}_3)_2$  and  $2(\text{CF}_3\text{SO}_3)_2$  with  $\text{CO}_2$  was monitored at 275 nm for the formation of  $[\{\text{Cu}_2(\text{Me2p})_2(\mu\text{-CO}_3)_2\}^{4+}$ , **4**, and at 330 nm for  $[\text{Cu}_2(\mu\text{-CO}_3)(\text{Me2m})]^{2+}$ , **5**, respectively, where a maximum change in absorbance occurs.

**Stopped-Flow Studies.** Stopped-flow kinetic measurements at ambient pressure were performed on a SX-18MV (Applied Photophysics) stopped-flow instrument. In a typical experiment, a buffer solution was mixed in varying volume ratios with tetraethylammonium bicarbonate,  $[\text{NET}_4][\text{HCO}_3]$ , in ACN in a gastight syringe. The  $[\text{NET}_4][\text{HCO}_3]$  solution was then rapidly mixed with the macrocyclic copper complexes in a 1:1 volume ratio in the stopped-flow apparatus. Kinetics of the reaction of  $1(\text{CF}_3\text{SO}_3)_2$  and  $2(\text{CF}_3\text{SO}_3)_2$  with  $[\text{NET}_4][\text{HCO}_3]$  was monitored at 322 and 330 nm for

**Table 1.** Crystal Data and Structure Refinement for **3**, **4**, **5**, **6**, and **8**

compound	<b>3</b>	<b>4</b>	<b>5</b>	<b>6</b>	<b>8</b>
empirical formula	C <sub>36</sub> H <sub>62</sub> Cl <sub>4</sub> Cu <sub>2</sub> N <sub>10</sub> O <sub>18</sub>	C <sub>79.50</sub> H <sub>118</sub> Cu <sub>4</sub> F <sub>12</sub> N <sub>19</sub> O <sub>18</sub> S <sub>4</sub>	C <sub>67</sub> H <sub>102</sub> Cl <sub>2</sub> Cu <sub>4</sub> F <sub>12</sub> N <sub>12</sub> O <sub>21</sub> S <sub>4</sub>	C <sub>70</sub> H <sub>112</sub> Cu <sub>4</sub> F <sub>12</sub> N <sub>14</sub> O <sub>21</sub> S <sub>4</sub>	C <sub>64</sub> H <sub>112</sub> Cl <sub>4</sub> Cu <sub>4</sub> N <sub>12</sub> O <sub>28</sub>
fw	1191.84	2238.33	2092.91	2096.12	1893.62
<i>T</i> (K)	298(2)	153(2)	153(2)	153(2) K	173(2)
$\lambda$ (Å)	0.71073	0.71073	0.71073	0.71073	0.71073
cryst syst	orthorhombic	monoclinic	monoclinic	triclinic	monoclinic
space group	<i>Pcca</i>	<i>C2/c</i>	<i>P2<sub>1</sub>/n</i>	<i>P1</i>	<i>P2<sub>1</sub>/n</i>
<i>a</i> (Å)	24.1931(9)	26.0381(7)	15.8738(7)	15.2221(6)	17.797(4)
<i>b</i> (Å)	11.7696(5)	13.1320(5)	15.7332(6)	17.3423(6)	13.879(2)
<i>c</i> (Å)	18.4880(6)	31.2787(12)	36.4668(16)	18.8869(7)	19.063(3)
$\alpha$	90°	90°	90°	91.036(2)°	90
$\beta$	90°	106.586(2)°	94.387(2)°	113.422(2)°	112.87(1)
$\gamma$	90°	90°	90°	103.114(2)°	90
<i>V</i> (Å <sup>3</sup> )	5264.3(3)	10250.2(6)	9080.7(7)	4422.9(3)	4338.6(1)
<i>Z</i>	4	4	4	2	2
$\rho_{\text{calc}}$ (Mg/m <sup>3</sup> )	1.504	1.450	1.531	1.574	1.449
abs coeff (mm <sup>-1</sup> )	1.087	0.992	1.171	1.144	1.170
<i>F</i> (000)	2472	4640	4312	2172	1976
cryst size (mm <sup>3</sup> )	0.35 × 0.20 × 0.10	0.20 × 0.20 × 0.03	0.08 × 0.08 × 0.06	0.05 × 0.05 × 0.05	0.40 × 0.25 × 0.05
$\theta$ range for data collection	1.68–25.03°	1.75–29.00°	1.41–31.55°	1.48–31.54°	1.33–25.10°
index ranges	–28 ≤ <i>h</i> ≤ 28, –12 ≤ <i>k</i> ≤ 14, –22 ≤ <i>l</i> ≤ 21	–35 ≤ <i>h</i> ≤ 35, –17 ≤ <i>k</i> ≤ 7, –28 ≤ <i>l</i> ≤ 42	–23 ≤ <i>h</i> ≤ 23, –22 ≤ <i>k</i> ≤ 22, –53 ≤ <i>l</i> ≤ 53	–21 ≤ <i>h</i> ≤ 18, –25 ≤ <i>k</i> ≤ 25, –27 ≤ <i>l</i> ≤ 27	–15 ≤ <i>h</i> ≤ 23, –18 ≤ <i>k</i> ≤ 18, –25 ≤ <i>l</i> ≤ 22
reflns collected	25 542	16094	136185	55 012	18 062
independent reflns	4655	11529	29181	26 983	7729
reflns	[ <i>R</i> (int) = 0.1066]	[ <i>R</i> (int) = 0.0598]	[ <i>R</i> (int) = 0.1969]	[ <i>R</i> (int) = 0.0896]	[ <i>R</i> (int) = 0.0515]
abs correction	SADABS (Siemens CCD)	SADABS (Bruker-Nonius)	SADABS (Bruker-Nonius)	SADABS (Bruker-Nonius)	SADABS (Siemens CCD)
refinement method			full-matrix least-squares on <i>F</i> <sup>2</sup>		
GOF on <i>F</i> <sup>2</sup>	1.179	0.926	0.908	0.858	1.157
final <i>R</i> indices	<i>R</i> 1 = 0.0696, w <i>R</i> 2 = 0.1440	<i>R</i> 1 = 0.0812, w <i>R</i> 2 = 0.1977	<i>R</i> 1 = 0.0888, w <i>R</i> 2 = 0.2131	<i>R</i> 1 = 0.0546, w <i>R</i> 2 = 0.1192	<i>R</i> 1 = 0.0857, w <i>R</i> 2 = 0.2143

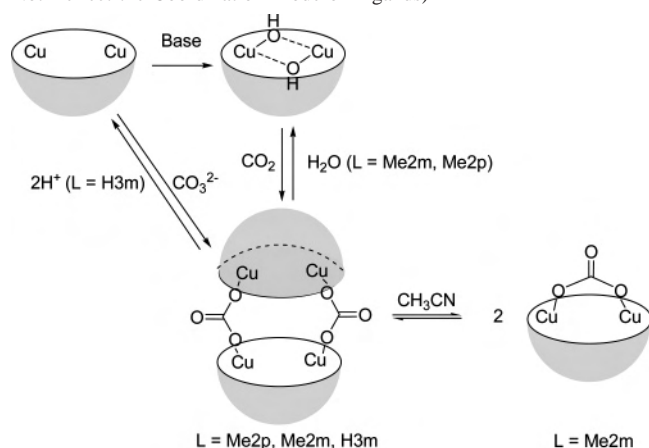
**Table 2.** Selected Bond Lengths (Å) and Bond Angles (deg) for **4**, **5**, **6**, and **8**

<b>4</b>	<b>5</b>	<b>6</b>	<b>6(cont)</b>	<b>8</b>
Cu1–O1 1.874(4)	Cu1B–O1B 1.920(4)	Cu1–O1 1.931(2)	Cu3–N8 2.015(3)	Cu1–O2 1.967(5)
Cu1–N2 1.990(4)	Cu1B–N2B 1.975(5)	Cu1–N2 2.022(3)	Cu3–N7 2.071(3)	Cu1–N2 2.008(6)
Cu1–N3 2.045(4)	Cu1B–N1B 2.124(5)	Cu1–N3 2.089(3)	Cu3–N9 2.082(3)	Cu1–N1 2.049(6)
Cu1–N1 2.1058(5)	Cu1B–N3B 2.147(5)	Cu1–N1 2.106(3)	Cu3–O3 2.210(2)	Cu1–N3 2.051(6)
Cu2–O2 1.873(4)	Cu1B–O3B 2.291(4)	Cu1–O7 2.229(2)	O2–Cu3 1.968(2)	Cu1–O1 2.331(5)
Cu2–N5 1.998(5)	Cu2B–O2B 1.927(4)	Cu2–O4 1.939(2)	Cu4–O5 1.949(2)	Cu1...Cu2 4.640(5)
Cu2–N4 2.052(4)	Cu2B–N5B 1.986(6)	Cu2–N5 2.038(3)	Cu4–N11 2.003(3)	Cu1...Cu2' 6.814(5)
Cu2–N6 2.068(5)	Cu2B–N6B 2.129(6)	Cu2–N4 2.093(3)	Cu4–N10 2.051(3)	Cu2–O3 1.971(5)
Cu1–Cu2 5.780	Cu2B–N4B 2.150(6)	Cu2–N6 2.104(3)	Cu4–N12 2.083(3)	Cu2–N5 1.999(6)
O1–Cu1–N2 167.04(16)	Cu2B–O3B 2.2777(4)	Cu2–O8 2.183(2)	Cu4–O6 2.237(2)	Cu2–N4 2.047(6)
O1–Cu1–N3 100.42(18)	Cu1B–Cu2B 4.514	O1–Cu1–N2 172.49(10)	O2–Cu3–N8 170.81(10)	Cu2–N6 2.056(6)
N2–Cu1–N3 85.69(19)	O2A–Cu2A–N5A 169.4(2)	O1–Cu1–N3 92.36(10)	O2–Cu3–N7 98.32(10)	Cu2–O1 2.368(5)
O1–Cu1–N1 92.42(18)	O2A–Cu2A–N6A 97.3(2)	N2–Cu1–N3 85.95(10)	N8–Cu3–N7 85.98(11)	O2–Cu1–N2 159.7(2)
N2–Cu1–N1 84.86(19)	N5A–Cu2A–N6A 86.9(2)	O1–Cu1–N1 93.04(10)	O2–Cu3–N9 94.13(10)	O2–Cu1–N1 88.4(2)
N3–Cu1–N1 160.46(17)	O2A–Cu2A–N4A 100.0(2)	N2–Cu1–N1 85.19(10)	N8–Cu3–N9 86.35(11)	N2–Cu1–N1 95.3(2)
O2–Cu2–N5 168.38(16)	N5A–Cu2A–N4A 85.7(2)	N3–Cu1–N1 152.49(10)	N7–Cu3–N9 147.54(11)	O2–Cu1–N3 95.1(2)
O2–Cu2–N4 93.63(19)	N6A–Cu2A–N4A 122.6(2)	O1–Cu1–O7 93.31(8)	O2–Cu3–O3 63.11(8)	N2–Cu1–N3 94.2(2)
N5–Cu2–N4 86.14(19)	O2A–Cu2A–O3A 63.15(16)	N2–Cu1–O7 94.21(9)	N8–Cu3–O3 107.93(10)	N1–Cu1–N3 142.0(2)
O2–Cu2–N6 98.1(2)	N5A–Cu2A–O3A 106.32(19)	N3–Cu1–O7 103.39(10)	N7–Cu3–O3 106.29(9)	O2–Cu1–O1 61.6(2)
N5–Cu2–N6 85.3(2)	N5A–Cu2A–O3A 119.55(19)	N1–Cu1–O7 103.20(9)	N9–Cu3–O3 106.09(9)	N2–Cu1–O1 98.3(2)
N4–Cu2–N6 161.24(17)	N4A–Cu2A–O3A 117.17(19)	O4–Cu2–N5 170.60(10)	O5–Cu4–N11 171.14(11)	N1–Cu1–O1 105.0(2)
	O1B–Cu1B–N1B 98.89(19)	O4–Cu2–N4 92.74(10)	O5–Cu4–N10 97.24(11)	N3–Cu1–O1 109.9(2)
	N2B–Cu1B–N1B 86.3(2)	N5–Cu2–N4 85.13(11)	N11–Cu4–N10 86.53(14)	O3–Cu2–N5 160.8(2)
	O1B–Cu1B–N3B 97.71(19)	O4–Cu2–N6 91.82(10)	O5–Cu4–N12 94.95(11)	O3–Cu2–N4 87.6(2)
	N2B–Cu1B–N3B 86.7(2)	N5–Cu2–N6 86.13(11)	N11–Cu4–N12 86.07(14)	N5–Cu2–N4 97.1(2)
	N1B–Cu1B–N3B 123.5(2)	N4–Cu2–N6 153.45(10)	N10–Cu4–N12 146.72(12)	O3–Cu2–N6 94.7(2)
	O1B–Cu1B–O3B 62.78(16)	O4–Cu2–O8 94.10(9)	O5–Cu4–O6 62.94(9)	N5–Cu2–N5 160.8(2)
	N2B–Cu1B–O3B 106.84(19)	N5–Cu2–O8 95.29(10)	N11–Cu4–O6 108.27(11)	N4–Cu2–N6 145.9(2)
	N1B–Cu1B–O3B 116.07(17)	N4–Cu2–O8 105.80(10)	N10–Cu4–O6 108.55(10)	O3–Cu2–O1 61.0(2)
	N3B–Cu1B–O3B 119.58(18)	N6–Cu2–O8 99.93(10)	N12–Cu4–O6 104.58(11)	N5–Cu2–O1 99.9(2)
				N4–Cu2–O1 101.1(2)

the formation of **4** and **5**, respectively, where large changes in absorbance are observed. All kinetic experiments were performed under pseudo-first-order conditions, i.e., with at least 10-fold excess of [NET<sub>4</sub>][HCO<sub>3</sub>] over **1**(CF<sub>3</sub>SO<sub>3</sub>)<sub>2</sub> and **2**(CF<sub>3</sub>SO<sub>3</sub>)<sub>2</sub>. Reported rate

constants are mean values of at least five kinetic runs, and the quoted uncertainties are based on the standard deviation. High-pressure stopped-flow experiments were performed at pressures up to 130 MPa on a custom-built instrument, described previously.<sup>33,34</sup>

**Scheme 2.** Preparation of the Cage Complexes (the Scheme Does Not Reflect the Coordination Mode of Ligands)



Kinetic traces were analyzed with the use of the OLIS KINFIT (Bogart, GA, 1989) set of programs.

## Results and Discussion

**Synthesis of the Complexes via  $\text{CO}_2$  Fixation.** Dinuclear hydroxo copper complexes of the general formula  $[\text{Cu}_2(\text{OH})_2(\text{L})]^{2+}$ , ( $\text{L} = \text{Me2p}$ , **1**;  $\text{L} = \text{Me2m}$ , **2**;  $\text{L} = \text{H3m}$ , **7**) where  $\text{L}$  is a hexaazamacrocyclic ligand (Schemes 1 and 2), react with  $\text{CO}_2$  to generate the carbonate complexes **4**( $\text{CF}_3\text{SO}_3$ )<sub>4</sub>, **5**( $\text{CF}_3\text{SO}_3$ )<sub>2</sub>, **6**( $\text{CF}_3\text{SO}_3$ )<sub>4</sub>, and **8**( $\text{ClO}_4$ )<sub>4</sub> (Scheme 2). The relative reactivity of the starting hydroxo complexes and the nuclearity of the species that are formed in this reaction appear to depend on the nature of the macrocyclic ligand. Hydroxocomplex **1** in ACN reacts very fast (reaction is complete in less than 0.5 min) with  $\text{CO}_2$  (1 atm), as monitored by UV–vis spectroscopy (vide infra), to generate **4**. The reaction of **2** with  $\text{CO}_2$  under analogous conditions to generate olive green **5** is significantly slower ( $t_{1/2} \approx 2$  min).

Unlike **1** and **2**, the putative hydroxide complex  $[\text{Cu}_2(\text{OH})_2(\text{H3m})]^{2+}$ , **7**, that forms upon addition of NaOH to  $[\text{Cu}_2(\text{H3m})(\text{CH}_3\text{CN})_4]^{4+}$ , **3**, could not be isolated because it undergoes a fast reaction with atmospheric  $\text{CO}_2$  to generate the tetranuclear box **8**. The high reactivity of **7** toward  $\text{CO}_2$  is remarkable since the reaction appears to be complete in less than 10 min in open air ( $\text{CO}_2$  concentration in air is 325 ppm).<sup>35</sup> In comparison, the modulated reactivity exhibited by the metal–hydroxide units in **1** and **2** most likely reflects a reduced nucleophilicity that may be traced to steric effects imposed by the methyl groups, the poorer donating abilities of the N-methylated groups in comparison with the secondary NH groups, which for the former results in nucleophilically deactivated OH groups,<sup>36,37</sup> or both.

Isolation of the dinuclear complex **5** requires strict anhydrous conditions since, in the presence of water, tetranuclear species **6** are isolated. Nevertheless, the latter rapidly reverts to **5** when dissolved in dry ACN, thus the initially blue solution ( $\lambda_{\text{max}} = 710$  nm) turns olive green ( $\lambda_{\text{max}} = 663$  and 798 nm) within seconds (see Figure S1). In addition, ESI-MS analysis of solutions prepared by dissolving **6** in ACN lack indication of the presence of the tetranuclear species in solution. This indicates that **6** is either present in small concentrations and fragile on the ESI experimental conditions or it is only stable in the solid state. In favor of the former, the broad feature between 600 and 700 nm in the UV–vis spectrum of **5** could indicate partial presence of **6** in solution. Carbonate species **4** and **6** can also be prepared by direct reaction in  $\text{CH}_3\text{CN}/\text{H}_2\text{O}$  10:1 v/v of the ligand,  $\text{Cu}(\text{CF}_3\text{SO}_3)_2$  and  $\text{Na}_2\text{CO}_3$  with a 1:2:1 molar ratio. Under these conditions, **5** could not be isolated. Unlike **6**, tetranuclear cages **4** and **8** appear to be stable in dry ACN solutions, as indicated by UV–vis spectroscopy and ESI-MS analysis (vide infra).

**Solid-State Structure Determination.** Data collection, solution, and refinement parameters are collected in Table 1, and selected bond lengths and angles of the structures are listed in Table 2. An ORTEP diagram of the cationic units of **4**, **5**, **6**, and **8** are displayed in Figure 1 (see Figure S2, Supporting Information, for structural details of **3**).

**4**( $\text{CF}_3\text{SO}_3$ )<sub>4</sub>. The cationic part of the molecule is composed of a dimer of macrocyclic complexes (Figure 1). Each of the two copper atoms is bridged through a carbonate group to a copper atom of a second macrocyclic unit, thus creating a molecular box. Copper atoms adopt a square planar coordination geometry defined by three N atoms from the macrocyclic ligand and an O atom from the carbonate group, which adopts an *anti-anti- $\mu$ - $\eta^1$ : $\eta^1$ - $\text{CO}_3$*  bridging mode (Scheme 3). Average Cu–N, Cu–O, and intramolecular Cu $\cdots$ Cu distances are 2.03, 1.87, and 6.72 Å, respectively, which are very similar to the corresponding distances 2.06, 1.85, and 6.71 Å found in the hydroxo precursor **1**( $\text{CF}_3\text{SO}_3$ )<sub>2</sub>,<sup>28</sup> indicating that the reaction causes significant structural changes neither in the coordination environment of the copper ion nor in the intramolecular Cu $\cdots$ Cu distance. Bond distances and angles are in concordance with Cu complexes with related coordination environments and indicate little distortion from a square planar geometry. Remarkably, a highly related structure has been recently reported by Martell et al. for the complex prepared from the non-methylated ligand H2p.<sup>38</sup>

**5**( $\text{ClO}_4$ )<sub>2</sub>. The crystallographic cell of compound **5**( $\text{ClO}_4$ )<sub>2</sub> contains two crystallographically nonequivalent cationic units (A and B), although their overall topology is identical and there is little variation in the respective structural parameters. Therefore, only the unit B will be described. Its X-ray analysis reveals a binuclear complex where the Cu ions are

(33) van Eldik, R.; Palmer, D. A.; Schmidt, R.; Kelm, H. *Inorg. Chim. Acta* **1981**, *50*, 131–135.

(34) van Eldik, R.; Gaede, W.; Wieland, S.; Kraft, J.; Spitzer, M.; Palmer, D. A. *Rev. Sci. Instrum.* **1993**, *64*, 1355–1357.

(35) Heicklen, J. *Atmospheric Chemistry*; Academic Press: New York, 1976; p 406.

(36) Golub, G.; Cohen, H.; Paoletti, P.; Bencini, A.; Messori, L.; Bertini, I.; Meyerstein, D. *J. Am. Chem. Soc.* **1995**, *117*, 8353–8361.

(37) Xifra, R.; Ribas, X.; Llobet, A.; Poater, A.; Duran, M.; Solà, M.; Stack, T. D. P.; Benet-Buchholz, J.; Donnadiou, B.; Mahía, J.; Parella, T. *Chem. Eur. J.* **2005**, *11*, 5146–5156.

(38) Gao, J.; Reibenspies, J. H.; Martell, A. E. *Inorg. Chim. Acta* **2002**, *338*, 157–164.

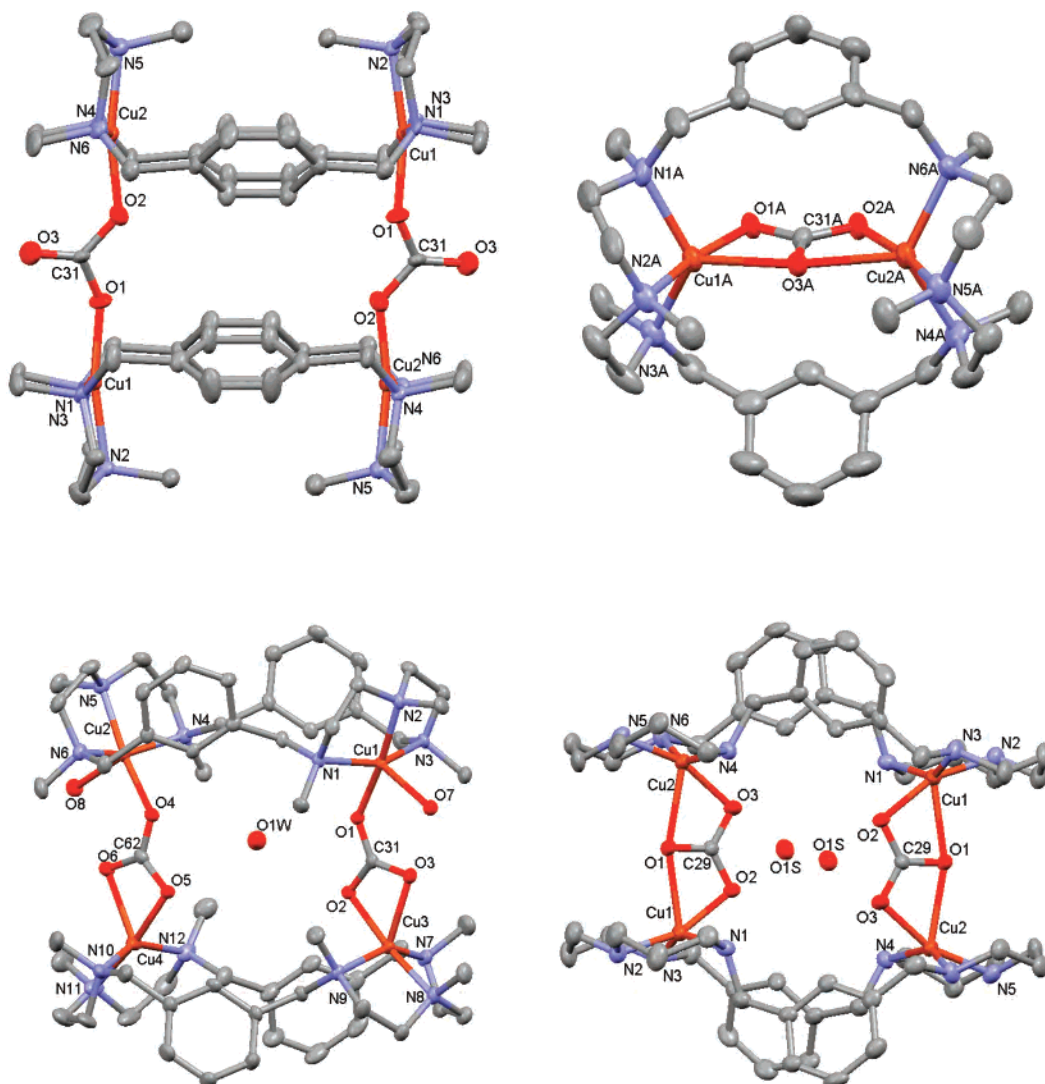
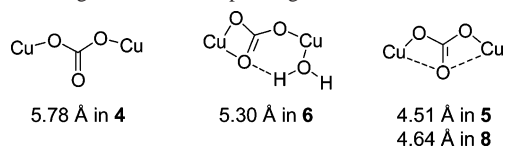


**Figure 1.** Crystal structure representation (ellipsoid 50%) of the cationic part of **4** (top left), **5** (top right), **6** (bottom left), and **8** (bottom right) (H atoms have been omitted for clarity).

**Scheme 3.** Binding Modes of the Carbonate Ligand in the Four Complexes along with the Corresponding Cu $\cdots$ Cu Distances



intramolecularly bridged by a carbonate molecule adopting the *anti-anti-μ-η<sup>2</sup>:η<sup>2</sup>* bridging mode (Scheme 3). The CO<sub>3</sub><sup>2-</sup> unit resides in the center of the hydrophobic cavity defined by the macrocycle, and it is pseudosymmetrically bound to the Cu atoms whose coordination geometry is best described as distorted trigonal bipyramidal ( $\tau = 0.78$ ).<sup>39</sup> Axial positions are occupied by the central N atom from the ligand and an O atom from the carbonate bridge at distances significantly shorter (1.98 and 1.92 Å *av*, respectively) than those observed for the equatorial Cu–N (2.14 Å *av*) and Cu–O (2.28 Å *av*) bonds. These structural parameters are in good accordance with reported Cu<sup>II</sup> complexes containing the same

geometry and ligand donor set.<sup>3</sup> Finally, the Cu $\cdots$ Cu distance is 4.51 Å. A comparison with its bis- $\mu$ -hydroxo precursor **2**(ClO<sub>4</sub>)<sub>2</sub> reveals that, unlike its *para*-substituted isomer, the reaction with CO<sub>2</sub> causes important changes in the complex as best evidenced by the lengthening of the Cu $\cdots$ Cu distance (3.0110(14) Å for **2**) and the different geometry adopted by the copper ions (square planar in **2**).<sup>28</sup>

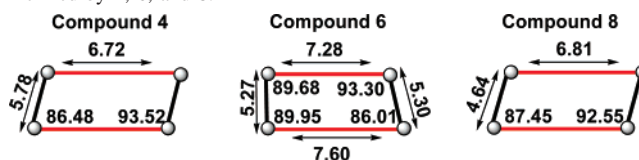
**6**(CF<sub>3</sub>SO<sub>3</sub>)<sub>4</sub>. On the other hand, complex **6**(CF<sub>3</sub>SO<sub>3</sub>)<sub>4</sub> is also an example of a tetranuclear complex resulting from the self-assembly of two dinuclear macrocyclic units (Figure 1). The solid-state structure is composed of a cationic unit, four triflate anions, and two ACN molecules. The cationic unit in turn contains two dinuclear macrocyclic copper complexes bridged by two carbonate ligands, giving rise to an internal cavity where there is a water molecule within hydrogen bond distance to four O atoms (3.013 Å < *d*<sub>O<sub>w</sub>–O<sub>CO3</sub> < 2.861 Å) from the carbonate ligands. The two carbonate ligands of each molecule adopt an *anti-anti-μ-η<sup>2</sup>:η<sup>1</sup>* bridging mode (Scheme 3), with an asymmetric ( $\Delta d_{\text{Cu–O}} \approx 0.26$  Å) bidentate chelate cycle. The two copper ions of each macrocyclic unit adopt the same coordination environ-</sub>

(39) Addison, A. W.; Rao, T. N.; Reedijk, J.; Van Rijn, J.; Verschoor, G. C. *J. Chem. Soc. Dalton Trans.* **1984**, 1349–1346.

ment, which in turn differs from the coordination geometries present on the second macrocycle. Thus, two of the copper ions bind to three N atoms of the macrocycle, an oxygen from the monodentate carbonate, and a water molecule, adopting a distorted square pyramidal ( $\tau = 0.28$  and  $0.33$ ) geometry. The coordinated water molecule occupies the apical position along an axially elongated axis (average Cu–O<sub>w</sub> = 2.206 Å) and appears to be H-bonded to the O-bound atom of the carbonate ligand (average O<sub>w</sub>–O<sub>CO3</sub> = 2.590 Å). This interaction fixes one of the H atoms such that it could be found and refined on the electron density maps. The coordination environment of the other two copper ions is formed by three N atoms of the macrocycle and two oxygen atoms of a bidentate chelate carbonate. The acute chelate angle imposed by the carbonate causes the coordination geometry to be intermediate between square planar and trigonal bipyramidal ( $\tau = 0.39$  and  $0.41$ ). While the two Cu···Cu distances associated with the carbonate-bridged copper ions are nearly identical (5.27(3) Å), intramacrocyclic Cu···Cu separations are less homogeneous, viz. 7.275 and 7.600 Å, respectively. Interestingly, these distances are nearly 3 and 4.5 Å longer than the ones measured in **2** and **5**, respectively, demonstrating that the Me2m cavity is highly flexible and capable of adapting to significantly different Cu···Cu distances. This is in sharp contrast with the structural properties of the Me2p macrocycle for which the Cu···Cu distance is uniformly maintained at 6.71(1) Å.

**8(ClO<sub>4</sub>)<sub>4</sub>.** The molecular structure of **8(ClO<sub>4</sub>)<sub>4</sub>** consists of a tetranuclear copper(II) complex with two H3m ligand molecules, two Cu atoms coordinated to N atoms of each ligand, and two carbonate groups acting as bridges between two copper centers from different ligands. Four perchlorate anions, four water, and two acetone molecules are present in the crystal cell. The molecule sits on a center of symmetry that transforms one macrocyclic ligand into the other. The ellipsoid drawing (Figure 1) shows that each copper metal atom is pentacoordinated to a N<sub>3</sub>O<sub>2</sub> ligand-donor set in a distorted square pyramidal geometry ( $\tau = 0.29$  for Cu1 and  $0.25$  for Cu2). Copper centers are coordinated to one O atom of the carbonate group and three N atoms to form the base of the pyramid, and a second O atom from the carbonate ligand resides in the axial position, along an axially elongated axis (Cu1–O1 2.33 Å, Cu2–O1 2.37 Å). The carbonate group is acting as a tridentate ligand adopting a *anti-anti-μ-η<sup>2</sup>:η<sup>2</sup>* binding mode (Scheme 3), with asymmetric bidentate coordination of the two O atoms of the copper-carbonate chelate ( $\Delta d_{\text{Cu-O}} \approx 0.38$  Å). Planes described by both carbonate groups are almost parallel with an angle between planes of 4.8°. The orientation of the carbonate groups toward the inside of the macrocycle allows the inclusion of two water molecules inside the rectangular box depicted. Each water molecule is H-bonded to O2 and O3 atoms of both carbonate group yielding four H-bonds ( $3.006$  Å <  $d_{\text{O}_w\text{-O}_{\text{CO}_3}}$  <  $3.243$  Å). Although the binding of the triamine arm to each Cu ion creates six-member chelate cycles in **8**, but five-member chelate cycles for **4**, **5**, and **6**, there appears to be a very small difference in the N<sub>2</sub>Cu chelate angles. Intra- and

**Scheme 4.** Schematic Representation of Hypothetical Quadrilaterals Defined by **4**, **6**, and **8**.<sup>a</sup>



<sup>a</sup> Bond distances (outside) and angles (inside) are obtained by considering Cu ions as vertex of the quadrilaterals (red lines refer to intramacrocyclic Cu···Cu distances, and black lines refer to Cu···Cu distances of CO<sub>3</sub><sup>2-</sup>-bridged atoms).

intermolecular Cu···Cu distances in **8** are 6.814(4) and 4.64(5) Å, respectively.

**Comparison between Self-Assembled Structures.** An overall estimation of the dimension of the self-assembled rectangular structures in **4**, **6**, and **8** can be made by considering a hypothetical quadrilateral with the Cu atoms occupying the four vertices (Scheme 4). Carbonate bridged Cu···Cu separation and intramacrocyclic Cu···Cu distances define the sides of the rectangle. Intermolecular Cu···Cu distances are determined by the coordination mode adopted by the carbonate bridge and are inversely related to its hapticity: 5.77(1) Å in **4(CF<sub>3</sub>SO<sub>3</sub>)<sub>4</sub>** (*anti-anti-μ-η<sup>1</sup>:η<sup>1</sup>*) > 5.27(3) Å in **6(CF<sub>3</sub>SO<sub>3</sub>)<sub>4</sub>** (*anti-anti-μ-η<sup>2</sup>:η<sup>1</sup>*) > 4.64(1) in **8(ClO<sub>4</sub>)<sub>4</sub>** (*anti-anti-μ-η<sup>2</sup>:η<sup>2</sup>*). Intramolecular Cu···Cu distances are surprisingly more homogeneous given the different structure of the three ligands employed in this work and range from 7.600/7.275(5) Å in **6(CF<sub>3</sub>SO<sub>3</sub>)<sub>4</sub>** to 6.814(5) Å in **8(ClO<sub>4</sub>)<sub>4</sub>** and 6.720(5) Å in **4(CF<sub>3</sub>SO<sub>3</sub>)<sub>4</sub>**. Finally, analysis of the angles in the Cu<sub>4</sub> quadrilaterals indicates only minor deviations from a hypothetical rectangle (86.01–93.52°). Space-filling models of **6** and **8** reveal that the orientation of the O atoms of the carbonate bridge toward the inside of the cavities creates small hydrophilic internal pockets, susceptible to be occupied by small polar molecules such as H<sub>2</sub>O, and indeed this is the case in **6** (one H<sub>2</sub>O, approximate spherical volume of 13 Å<sup>3</sup>) and **8** (two H<sub>2</sub>O molecules placed at both sides of the rectangle, approximate spherical volume of 13 Å<sup>3</sup> each). On the other hand, in **4(CF<sub>3</sub>SO<sub>3</sub>)<sub>4</sub>**, the relative orientation of the aromatic rings and the carbonate bridges, toward the inside and outside of the cavity, respectively, renders a small empty hydrophobic cavity. It should be pointed out that macrocyclic complexes containing meta-substituted aromatic rings Me2m and H3m appear to exhibit a range of Cu···Cu distances depending on the linker molecule bound to the copper ions (*vide supra*).

**Spectroscopic Properties.** A summary of the spectroscopic properties of the complexes described in this work is collected in Table 3. FT-IR spectra of the carbonate compounds show for each case two intense features between 1550 and 1330 cm<sup>-1</sup> associated with CO<sub>3</sub><sup>2-</sup> symmetric and antisymmetric stretching modes, respectively.<sup>40</sup>

The UV–vis spectra of the complexes prepared in this work (Table 3) exhibit intense absorptions below 400 nm arising from ligand π–π\* and ligand-to-metal charge-transfer

(40) Nakamoto, K. *Infrared and Raman Spectra of Inorganic and Coordination Compounds*, 4th ed.; John Wiley: New York, 1986; pp 252–254.

**Table 3.** Spectroscopic and Magnetic Properties of Complexes **4**, **5**, **6**, and **8**

	<b>4</b>	<b>5</b>	<b>6</b>	<b>8</b>
$\nu_{\text{CO}_3}$ (cm <sup>-1</sup> )	1543, 1335	1497, 1405	1491, 1387	1486, 1452
$\lambda_{\text{max}}$ (nm)	209 (5490)	287 (9000)	293, 710	266 (14 700)
$\epsilon$ (mol <sup>-1</sup> dm <sup>3</sup> cm <sup>-1</sup> )	285 (2250)	381 (3200)		370 (sh, 2570), 676 (1310)
	504 (645)	663 sh (610)		
	641 (680)	798 (930)		
$J$ (cm <sup>-1</sup> )	-23.1	n.m. <sup>a</sup>	-108.3	-163.4
$g$	2.14		2.19	2.24

<sup>a</sup> n.m. = not measured.

transitions, but most interestingly, they present weak features between 500 and 800 nm attributed to ligand field transitions, characteristic of a Cu<sup>II</sup> (d<sup>9</sup>) ion. The energy and number of these transitions convey information about the coordination geometry of the copper ions in the complexes. Square planar geometries present in **1** and **4** are characterized by a double-hump at 504 and 641 nm responsible for the gray-blue color of their solutions. On the other hand, the square pyramidal coordination geometry adopted by the Cu ion in **2**, **6**, and **8** give rise to deep blue solutions ( $\lambda_{\text{max}} = 624, 710,$  and  $676$  nm, respectively). This contrasts with the green-yellow color exhibited by **5**, arising from a relatively strong absorption in the near-IR region ( $\lambda_{\text{max}} = 798$  nm,  $\epsilon = 930$  M<sup>-1</sup> cm<sup>-1</sup>). Interestingly, the latter compound is also the only one where the Cu ions adopt clearly defined trigonal bipyramidal geometries ( $\tau = 0.78$ ). Although an accurate study of the number of bands underlying each of these low-energy features and the associated transitions is complicated and beyond the scope of this study, the UV-vis spectra of the complexes in ACN suggest that, with the single exception of **6**, the solid-state coordination geometries are retained in solution.<sup>41</sup> In addition, the bathochromic shift of the ligand field transitions upon changing from a square pyramidal toward a trigonal bipyramidal geometry is in good accordance with the spectrochemical behavior associated with copper complexes containing tripodal amine ligands.<sup>42,43</sup>

**Structure in Solution. ESI-MS Analysis.** Electrospray MS analysis turns out to be a valuable method to test the integrity of the tetranuclear cage complexes in solution (Figure S3). Thus, ACN solutions of **4**(CF<sub>3</sub>SO<sub>3</sub>)<sub>4</sub> and **8**(ClO<sub>4</sub>)<sub>4</sub> reveal cluster ions at  $m/z = 831$  and  $1605$ , respectively, with an isotopic pattern best described as  $[[\{\text{Cu}_2(\text{Me}_2\text{p})\}_2(\text{CO}_3)_2](\text{CF}_3\text{SO}_3)_2]^{2+}$  and  $[[\{\text{Cu}_2(\text{H}_3\text{m})\}_2(\text{CO}_3)_2](\text{ClO}_4)_3]^{+}$ , respectively, indicating that the tetrameric structure is retained in solution. On the other hand, solutions of **5**(CF<sub>3</sub>SO<sub>3</sub>)<sub>4</sub> and **6**(CF<sub>3</sub>SO<sub>3</sub>)<sub>4</sub> appear to show identical ESI-MS spectra, with cluster ions at  $m/z = 831$ , but showing isotopic patterns consistent with a  $[[\{\text{Cu}_2(\text{Me}_2\text{m})(\text{CO}_3)\}(\text{CF}_3\text{SO}_3)]^{+}$  formulation. This suggests that the solid-state tetranuclear structure found in **6** is not retained in solution or, alternatively, the tetranuclear core dissociates under ESI conditions.

(41) Hathaway, B. J.; Billing, D. E. *Coord. Chem. Rev.* **1970**, *5*, 143–207.

(42) Schatz, M.; Becker, M.; Thaler, F.; Hampel, F.; Schindler, S.; Jacobson, R. R.; Tyeklar, Z.; Murthy, N. N.; Ghosh, P.; Chen, Q.; Zubieta, J.; Karlin, K. D. *Inorg. Chem.* **2001**, *40*, 2312–2322.

(43) Dittler-Klingemann, A. M.; Orvig, C.; Hahn, F. E.; Thaler, F.; Hubbard, C. D.; van Eldik, R.; Schindler, S.; Fabian, I. *Inorg. Chem.* **1996**, *35*, 7798–7803.

**Magnetic Properties.**  $\chi_{\text{M}}T$  vs  $T$  plots measured in the range 4–300 K for complexes **4**(CF<sub>3</sub>SO<sub>3</sub>)<sub>4</sub>·8H<sub>2</sub>O, **6**(CF<sub>3</sub>SO<sub>3</sub>)<sub>4</sub>·4H<sub>2</sub>O, and **8**(ClO<sub>4</sub>)<sub>2</sub>·6H<sub>2</sub>O·CH<sub>3</sub>COCH<sub>3</sub> are collected as Supporting Information (Figures S4–S6), and coupling constants,  $J$ , and  $g$  values derived from fitting of the data are shown in Table 3. Compound **5** was not studied because it was not possible to obtain sufficient amount of pure product to prepare a sample for magnetic measurements.

In the three cases,  $\chi_{\text{M}}T$  decreases upon cooling, tending to a zero value at low temperatures, indicating that antiferromagnetic interactions dominate. In these tetranuclear complexes, the Cu<sup>II</sup> ions show a rectangular disposition, with Cu<sup>II</sup> ions bridged through the macrocyclic ligand and Cu<sup>II</sup> ions bridged by a carbonate ligand. The metallic centers bridged by the macrocyclic ligand show a long Cu···Cu distance ( $\sim 7$  Å), and furthermore, this ligand does not furnish a good path for the magnetic interaction. Therefore, the magnetic properties of these compounds will be attributed to the Cu<sup>II</sup>···Cu<sup>II</sup> interaction through the carbonate bridging ligand, and from the magnetic point of view, the tetranuclear complex may be considered as constituted by two equivalent dinuclear complexes. So, in all cases, fitting of the data was done with the Bleaney–Bowers expression<sup>44</sup> for a Cu<sup>II</sup> dinuclear complex with paramagnetic impurities. Coupling constants derived from fitting the data to the Hamiltonian  $H = -JS_1S_2$  are  $J = -23.1$  cm<sup>-1</sup>,  $g = 2.14$  for **4**,  $J = -108.3$  cm<sup>-1</sup>,  $g = 2.19$  for **6**, and  $J = -163.4$  cm<sup>-1</sup>,  $g = 2.24$  for **8**.

Magnetic coupling via a carbonate bridge, due to its ability to bridge in a variety of coordination modes, can afford a wide range of magnetic behaviors, from strong antiferromagnetic coupling to even weak ferromagnetic coupling.<sup>3</sup> Compound **4** exhibits a square planar geometry around each Cu<sup>II</sup> with only one O atom of the carbonate group coordinated to the metal, adopting an *anti-anti-μ-η<sup>1</sup>:η<sup>1</sup>-CO<sub>3</sub>* bridging mode. The two coordination planes of the Cu<sup>II</sup> ions are almost coplanar and almost perpendicular to the plane containing the carbonate, and the non-coordinated oxygen atom of the carbonate ligand is at long distance from the metallic centers (3.4 Å). Therefore, this coordination mode excludes the possibility of a pseudo-oxo superexchange pathway, and only allows magnetic coupling through an anti–anti superexchange pathway.

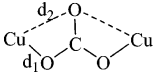
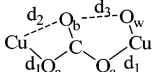
In compound **8**, the Cu<sup>II</sup> ions are in a distorted square pyramidal environment, with one oxygen atom of the carbonate ligand in the basal plane, bridging the Cu<sup>II</sup> ions in an anti–anti mode. A second oxygen atom is at  $\sim 2.4$  Å, in the apical position of the polyhedra. Therefore, the carbonate ligand shows an *anti-anti-μ-η<sup>2</sup>:η<sup>2</sup>-CO<sub>3</sub>* bridging mode, and in this case, in addition to the magnetic pathway through the anti–anti carbonate ligand, there is the pathway through the pseudo-oxo ligand.

Table 4 summarizes the structural parameters of published compounds with the same interaction path as **4** and **8**. All these compounds show one oxygen atom of the carbonate ligand at  $d_1$  distance, in the basal plane, and the oxygen atom

(44) Bleaney, B.; Bowers K. D. *Proc. R. Soc. London* **1952**, *A214*, 451.



**Table 4.** Magnetic Coupling  $J$  Values and Relevant Structural Parameters for **4**, **6**, **8**, and Structurally Related Dinuclear  $\text{Cu}^{\text{II}}$  Complexes with a Symmetric and Asymmetric Bridging Carbonate Moiety<sup>a</sup>

		$J$ ( $\text{cm}^{-1}$ )	$d_1$ ( $\text{\AA}$ )	$d_2$ ( $\text{\AA}$ )	$d(\text{Cu}\cdots\text{Cu})$ ( $\text{\AA}$ )	ref
<b>4</b>		-23.1	1.87	3.4	5.78	this work
<b>8</b>		-163.4	1.97	2.35	4.64	this work
$[\{\text{Cu}(\text{dpyam})_2\}_2(\mu\text{-CO}_3)]^{2+}$		-90.4	1.97	2.95	5.56	48
$[\{\text{Cu}(\text{bpy})_2\}_2(\mu\text{-CO}_3)]^{2+}$		-140.4	1.95	2.32	5.26	49
$[\{\text{Cu}(\text{Et}_5\text{dien})\}_2(\mu\text{-CO}_3)]^{2+}$		-207	1.95	2.33	4.55	50
		$J$ ( $\text{cm}^{-1}$ )	$d_1$ ( $\text{\AA}$ )	$d_2$ ( $\text{\AA}$ )	$d_3$ ( $\text{\AA}$ )	ref
<b>6</b>		-108.3	1.95	2.23	2.59	this work
$[\{\text{Cu}(\text{Et}_4\text{dien})\}_2(\mu\text{-CO}_3)\{\text{Cu}(\text{H}_2\text{O})(\text{Et}_4\text{dien})\}]^{2+}$		-17.8	2.28	1.98	2.68	3

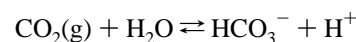
<sup>a</sup> dpyam = di-2-pyridylamine; Et<sub>5</sub>dien = *N,N,N',N'',N'''*-pentaethylbis(2-aminoethane)amine; Et<sub>4</sub>dien = *N,N,N'',N'''*-tetraethylbis(2-aminoethane)amine.

at  $d_2$  distance, in apical position. As was mentioned,  $d_2$  for compound **4** is larger than for the other compounds, and the magnetic interaction is only due to the anti-anti pathway of the carbonate bridge. Consequently, the magnetic interaction for this compound is weaker than for the others. The compound with dpyam ligand (Table 4) shows an intermediate situation, while compound **8**, as well as complexes with bpy and Et<sub>5</sub>dien ligands, shows important antiferromagnetic couplings. In these compounds, in spite of the apical position of the pseudo-oxo bridging ligand, the distortion of the square-pyramid toward the bipyramidal geometry allows the interaction through the pseudo-oxo pathway, and consequently, the antiferromagnetic interaction increases.

The pathway of the magnetic interaction on compound **6** is quite different. The carbonate ligand is coordinated in an asymmetric *anti-anti- $\mu$ - $\eta^2$ : $\eta^1$ -CO<sub>3</sub>* bridging mode, and the copper(II) ions are not equivalent. One of them shows in the apical position one oxygen atom of the carbonate bridging ligand ( $\text{O}_b$ ), while the other  $\text{Cu}^{\text{II}}$  ion shows in the apical position one water molecule ( $\text{O}_w$ ). The other two oxygen atoms of the carbonate bridging ligand ( $\text{O}_a$ ) are in the basal planes of the square pyramid around each  $\text{Cu}^{\text{II}}$  ion. Moreover, there are hydrogen-bond interactions between the  $\text{O}_w$  and  $\text{O}_b$ . A similar compound was reported in the literature, where the Et<sub>4</sub>dien ligand was used,  $[\{\text{Cu}(\text{Et}_4\text{dien})\}_2(\mu\text{-CO}_3)\{\text{Cu}(\text{H}_2\text{O})(\text{Et}_4\text{dien})\}]^{2+}$ .<sup>3</sup> However, in this compound, the antiferromagnetic interaction is weaker than for compound **6** (Table 4). Both compounds have two pathways for the magnetic interaction through the carbonate bridging ligand: the anti-anti coordination mode ( $\text{O}_a$ ,  $\text{O}_a$ ) and the syn-anti coordination mode ( $\text{O}_b$ ,  $\text{O}_b$ ). Comparison of the structural data indicate that for **6**  $d_1 < d_2$ , while for the complex with Et<sub>4</sub>dien  $d_1 > d_2$ . On the other hand, the geometry around the  $\text{Cu}^{\text{II}}$  ions in the complex with Et<sub>4</sub>dien is trigonal bipyramidal, with the  $d_{z^2}$  orbital pointing to the  $\text{O}_b$  atom, while for **6**, is a distorted square pyramid, with the  $d_{x^2-y^2}$  orbital pointing to the  $\text{O}_a$  atom. Therefore, the most important pathway for the magnetic interaction on compound **6** is the anti-anti coordination mode ( $\text{O}_a$ ,  $\text{O}_a$ ) (antiferromagnetic contribution), while for  $[\{\text{Cu}(\text{Et}_4\text{dien})\}_2(\mu\text{-CO}_3)\{\text{Cu}(\text{H}_2\text{O})(\text{Et}_4\text{dien})\}]^{2+}$  it is the syn-anti coordination mode ( $\text{O}_b$ ,  $\text{O}_a$ ) (ferromagnetic

contribution). This fact could explain the most antiferromagnetic coupling observed for compound **6** comparatively to the compound with Et<sub>4</sub>dien ligand.

**Kinetic Studies on the Binding of CO<sub>2</sub>.** A series of preliminary kinetic studies were performed as part of this study in order to follow the binding of CO<sub>2</sub> to the  $\text{Cu}^{\text{II}}$  complexes by UV-vis spectrophotometry under the conditions employed in the synthesis of the isolated complexes (an account of the preliminary studies is given in the Supporting Information). In general, the observed reactions were kinetically not clean reactions and depended strongly on the water content of the solvent. The results suggested that this can be related to the spontaneous hydration of CO<sub>2</sub> to form  $\text{HCO}_3^-$  (see reaction given below), which will depend on the water content of the solvent and that it is actually  $\text{HCO}_3^-$  that reacts with the complexes to form the isolated carbonate complexes instead of dissolved CO<sub>2</sub>.



In order to test this,  $[\text{NET}_4][\text{HCO}_3]$  was used as a source for  $\text{HCO}_3^-$  and the reactions with **1**(CF<sub>3</sub>SO<sub>3</sub>)<sub>2</sub> and **2**(CF<sub>3</sub>SO<sub>3</sub>)<sub>2</sub> were studied in pure ACN in the absence and presence of water. The observed spectral changes indicated that the reaction with  $[\text{NET}_4][\text{HCO}_3]$  is much faster than the reaction with dissolved CO<sub>2</sub> and that the conversion to the corresponding carbonate complexes **4** and **5** is almost complete under these conditions (see Figures S12 and S13, respectively). Typical kinetic traces recorded for the reaction of **2**(CF<sub>3</sub>SO<sub>3</sub>)<sub>2</sub> with  $\text{HCO}_3^-$  in the presence of water showed a rapid formation of the carbonate complex followed by a subsequent slow reaction as illustrated in Figure 2. Both reaction steps show a dependence on the  $\text{HCO}_3^-$  concentration as reported in Figure S14.

To prevent the complications that arise in the presence of water (see Supporting Information), we studied both reaction systems in pure ACN as solvent and  $[\text{NET}_4][\text{HCO}_3]$  as source for  $\text{HCO}_3^-$  using stopped-flow techniques. The formation of **4** clearly showed two steps, and the kinetic traces had to be fitted with a double exponential function (see Figure S12) of which the first reaction step accounted for the major part

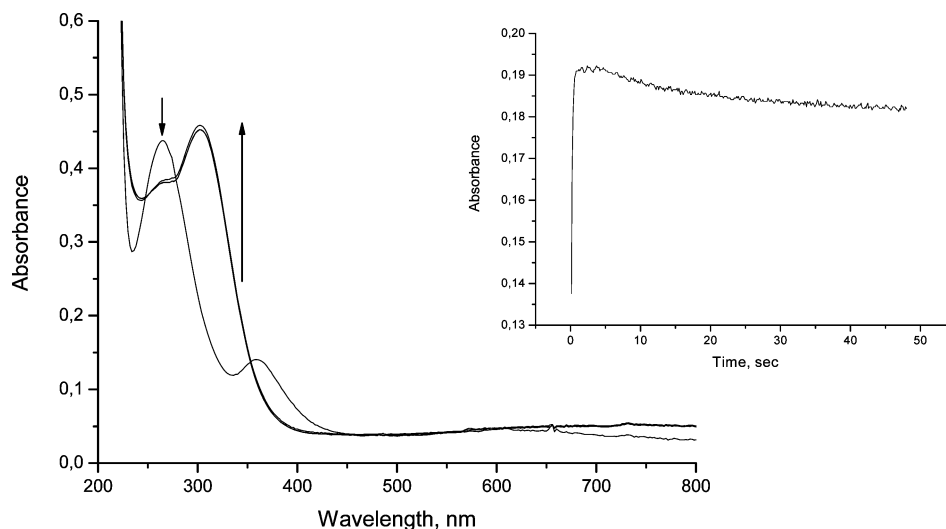


**Figure 2.** Spectral changes observed for the reaction of  $[\text{Cu}_2(\mu\text{-OH})_2(\text{Me2m})]^{2+}$ , **2**, with  $\text{HCO}_3^-$  in the presence of water. A typical kinetic trace measured at 315 nm is shown in the inset. Experimental conditions:  $[\text{Cu}_2(\mu\text{-OH})_2(\text{Me2m})](\text{CF}_3\text{SO}_3)_2 = 0.25$  mM,  $[\text{NEt}_4][\text{HCO}_3] = 5$  mM,  $\lambda_{\text{det}} = 315$  nm,  $T = 25$  °C,  $\text{ACN}/\text{H}_2\text{O} = 9:1$  (10%  $\text{H}_2\text{O}$ ).

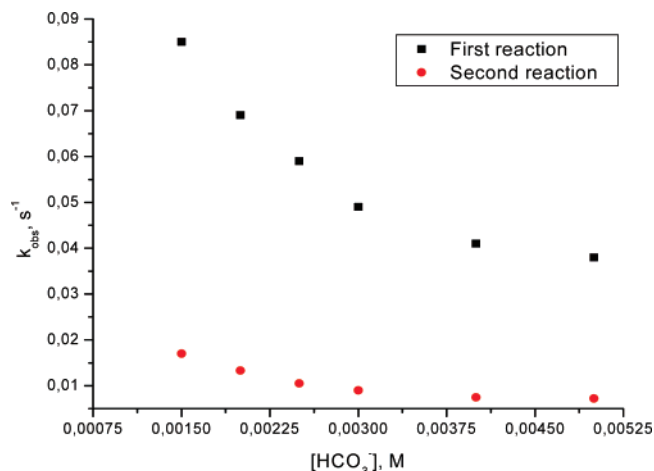
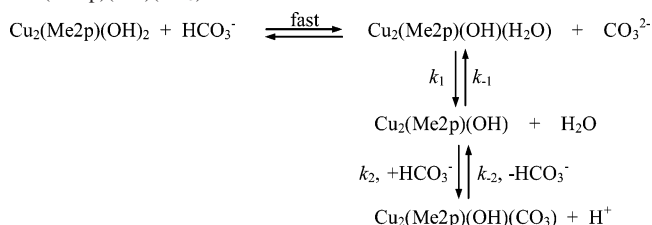


**Figure 3.** Plots of  $k_{\text{obs}}$  versus  $[\text{HCO}_3^-]$  for the reaction of  $[\text{Cu}_2(\text{OH})_2(\text{Me2p})]^{2+}$ , **1**, with  $\text{HCO}_3^-$ . Experimental conditions:  $[\text{Cu}_2(\text{OH})_2(\text{Me2p})](\text{CF}_3\text{SO}_3)_2 = 0.15$  mM,  $\lambda_{\text{det}} = 322$  nm, in pure ACN at 5 °C.

of the observed spectral changes. The kinetics of the two steps could be resolved in a limited low-temperature range and showed a decrease in the observed rate constant for both reaction steps as a function of the  $\text{HCO}_3^-$  concentration, as shown in Figure 3. Such an unusual kinetic behavior has been reported for substitution processes before<sup>45</sup> and suggests that the overall process involves the reversible formation and decay of a steady-state intermediate. In the present case we suggest that both observed reaction steps follow the type of mechanism depicted in Scheme 5. This involves the rapid labilization of coordinated hydroxide through protonation by bicarbonate in a pre-equilibrium, followed by rate-determining reversible dissociation of coordinated water to form a steady-state intermediate that reversibly binds bicarbonate in the subsequent step. A similar mechanism can account for the observed kinetic behavior of the second reaction step in terms of the displacement of the second hydroxy ligand. When a steady-state approximation is applied to the  $\text{Cu}_2$ -

**Scheme 5.** Suggested Reaction Scheme for the Formation of  $\text{Cu}_2(\text{Me2p})(\text{OH})(\text{CO}_3)$



(Me2p)(OH) intermediate in Scheme 5, the expression for the observed rate constant is given by<sup>45</sup>

$$k_{\text{obs}} = \frac{k_1 k_2 [\text{HCO}_3^-] + k_{-1} k_{-2}}{k_{-1} + k_2 [\text{HCO}_3^-]}$$

which at high  $\text{HCO}_3^-$  concentration reduces to  $k_{\text{obs}} = k_1$ , i.e., dissociation of water from  $\text{Cu}_2(\text{Me2p})(\text{OH})(\text{H}_2\text{O})$  is the rate-determining step, and at low  $\text{HCO}_3^-$  concentration reduces to  $k_{\text{obs}} = k_{-2}$ , i.e., dissociation of bicarbonate is the rate-determining step for the back reaction. The unusual concentration dependence observed in Figure 3 originates from the fact that  $k_{-2} > k_1$ , i.e., we are dealing with an efficient back reaction.<sup>45</sup> The temperature and pressure dependences of the first (major) reaction step at high  $\text{HCO}_3^-$  concentration, i.e., where  $k_{\text{obs}} = k_1$ , are reported in Figures 4 and S15, from which the following activation parameters were calculated, viz.  $\Delta H^\ddagger = 93 \pm 4$  kJ mol<sup>-1</sup>,  $\Delta S^\ddagger = +64 \pm 15$  J mol<sup>-1</sup> K<sup>-1</sup>, and  $\Delta V^\ddagger = +20 \pm 3$  cm<sup>3</sup> mol<sup>-1</sup> at 10 °C. In particular, the significantly positive activation entropy and volume values support the suggested dissociation of coordinated water as the rate-determining step ( $k_1$ ) to account for the bicarbonate concentration dependence observed in Figure 3 for both reaction steps, which are suggested to follow the same mechanism. The possible participation of monomeric species of **1** could be excluded on the basis that the kinetic data for both reaction steps at a fixed  $\text{HCO}_3^-$  concentration did not show any significant dependence on the complex concentration over the range 0.075–0.30 mM.

(45) Malin, J. M.; Toma, H. E.; Giesbrecht, E. J. *Chem. Educ.* **1977**, *54*, 385–386.

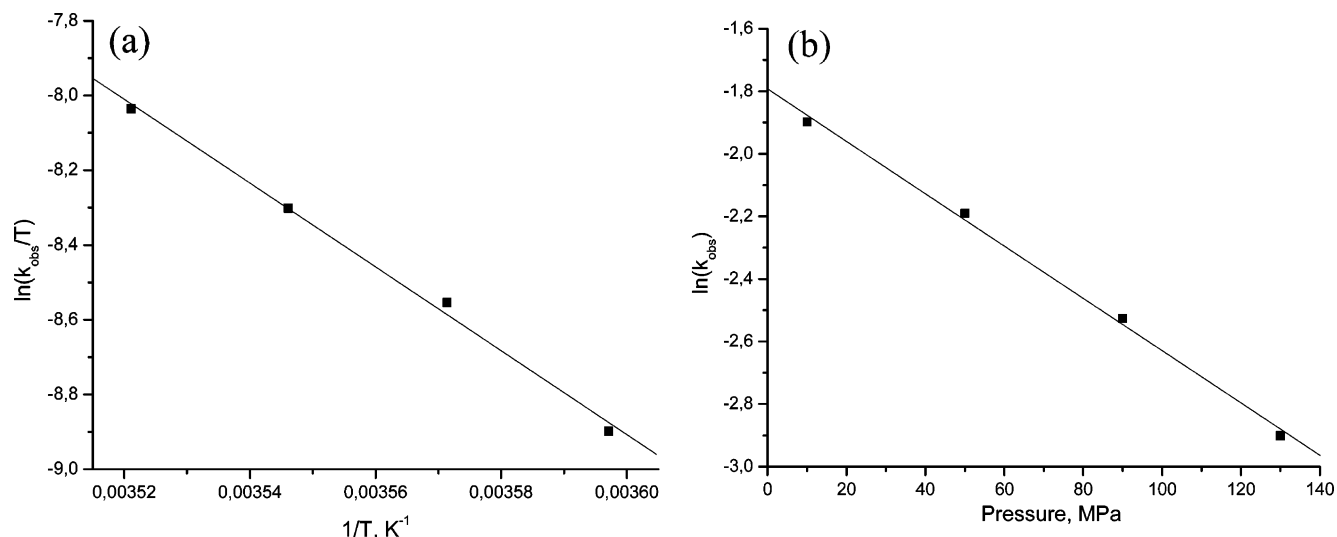


**Figure 4.** (a) Temperature dependence of the reaction of  $[\text{Cu}_2(\text{OH})_2(\text{Me2p})]^{2+}$ , **1**, with  $\text{HCO}_3^-$ . (b) Pressure dependence of the reaction at 10 °C. Experimental conditions:  $[\text{Cu}_2(\text{OH})_2(\text{Me2p})](\text{CF}_3\text{SO}_3)_2 = 0.15$  mM,  $[\text{NEt}_4][\text{HCO}_3] = 5$  mM,  $\lambda_{\text{det}} = 322$  nm, in pure ACN.

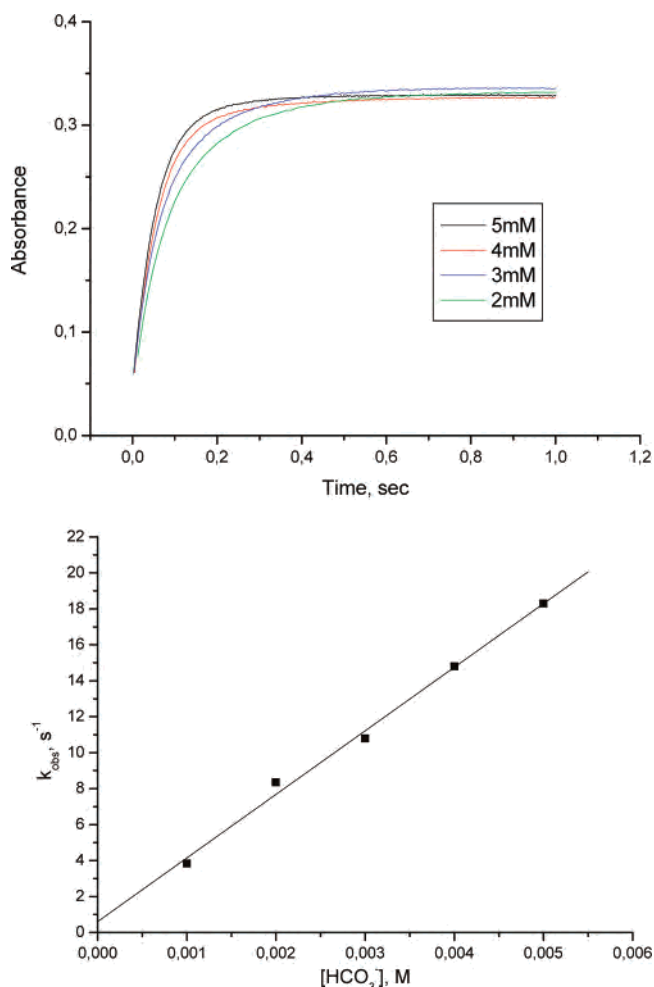


**Figure 5.** Effect of  $[\text{HCO}_3^-]$  on the reaction with  $[\text{Cu}_2(\mu\text{-OH})_2(\text{Me2m})]^{2+}$ , **2**. Top: Kinetic traces recorded as a function of  $[\text{HCO}_3^-]$ . Bottom: Plot of  $k_{\text{obs}}$  versus  $[\text{HCO}_3^-]$ . Experimental conditions:  $[\text{Cu}_2(\mu\text{-OH})_2(\text{Me2m})](\text{CF}_3\text{-SO}_3)_2 = 0.28$  mM,  $\lambda_{\text{det}} = 330$  nm,  $T = 25$  °C, in pure ACN.

The formation of the carbonate complex **5** exhibited perfect first-order behavior in the presence of an excess of  $\text{HCO}_3^-$  (see Figure 5). The second-order rate constant calculated from the data in Figure 5 is  $(3.5 \pm 0.1) \times 10^3$

$\text{M}^{-1} \text{s}^{-1}$  at 25 °C. The temperature and pressure dependencies of the reaction in pure ACN are reported in Figure 6 from which the following activation parameters for the second-order rate constant ( $k_{\text{on}}$ ) were calculated:  $\Delta H^\ddagger = 73 \pm 2$  kJ mol $^{-1}$ ,  $\Delta S^\ddagger = +24 \pm 7$  J mol $^{-1}$  K $^{-1}$ , and  $\Delta V^\ddagger = +9.6 \pm 0.1$  cm $^3$  mol $^{-1}$  at 5 °C. The activation entropy and activation volume data suggest that the coordination of  $\text{HCO}_3^-$  to the  $\text{Cu}^{\text{II}}$  complex **2** also follows a dissociative mechanism and most probably involves protonation of coordinated hydroxide by  $\text{HCO}_3^-$ , followed by the release of the labile water molecule prior to bond formation with  $\text{HCO}_3^-$ , as suggested in Scheme 5. This process can be visualized as a concerted interaction between both bridging hydroxyl ligands and bicarbonate and is suggested to have a dissociative interchange character based on the less positive activation volume found for this reaction as compared to that found for the reaction with complex **1**. The possible participation of monomeric species of **2** could be excluded on the basis that the kinetic data for at a fixed  $\text{HCO}_3^-$  concentration did not show any significant dependence on the complex concentration over the range 0.075–0.30 mM.

A qualitative comparison of the observed rate constants for the binding of bicarbonate to **1** and **2** shows that the reaction with **2** is faster than with **1**, by a factor of  $\sim 10$  when the difference in temperature (25 vs 5 °C) is taken into account. This is only a rough estimate as a result of the different bicarbonate concentration dependencies reported for the complexes in Figures 3 and 5. The observed trend is ascribed to the more effective interaction between both bridging hydroxy ligands in **2** with bicarbonate than in **1**. Furthermore, in the case of **1**, two similar reaction steps were observed as a result of both hydroxy ligands being displaced by bicarbonate in two subsequent dissociative processes that involve the formation of coordinatively unsaturated intermediates. This is not the case for the binding of bicarbonate to **2** which occurs as a single-step process. Thus, the nature of the coordinated hydroxy ligands, i.e., bridging versus

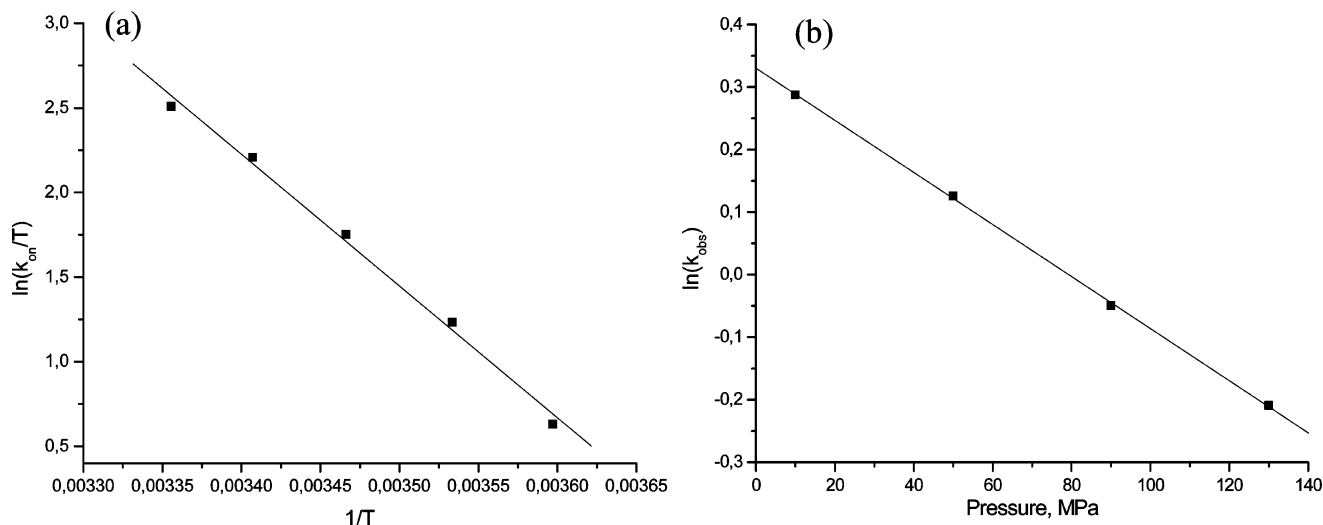


**Figure 6.** (a) Temperature dependence of the reaction of  $[\text{Cu}_2(\mu\text{-OH})_2(\text{Me2m})]^{2+}$ , **2**, with  $\text{HCO}_3^-$ . (b) Pressure dependence of the reaction at 5 °C. Experimental conditions:  $[\text{Cu}_2(\mu\text{-OH})_2(\text{Me2m})](\text{CF}_3\text{SO}_3)_2 = 0.28$  mM,  $[\text{NEt}_4][\text{HCO}_3] = 3$  mM,  $\lambda_{\text{det}} = 330$  nm, in pure ACN.

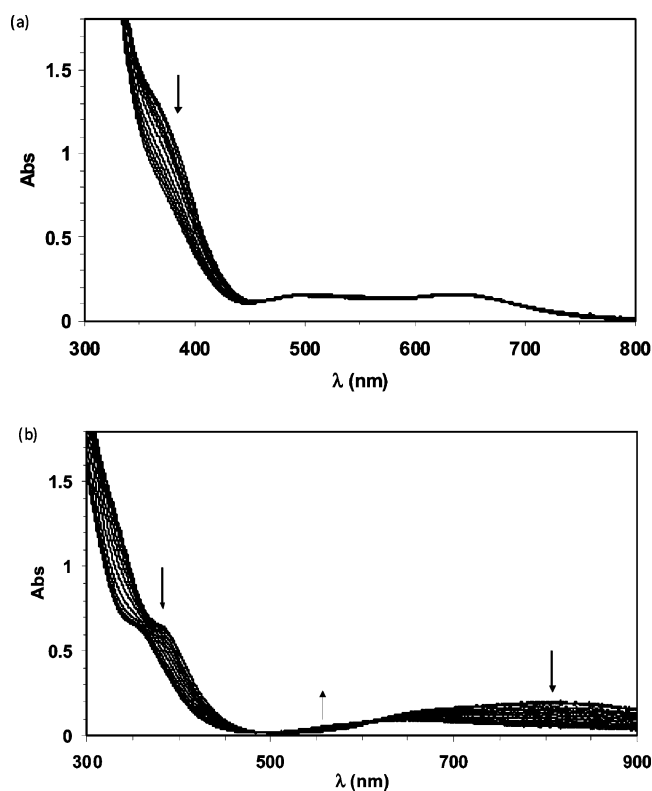


**Figure 7.** UV-vis spectral changes observed when (a) a 0.21 mM solution of **4** in ACN under a N<sub>2</sub> atmosphere releases CO<sub>2</sub>(g) to generate  $[\text{Cu}_2(\text{OH})_2(\text{Me2p})]^{2+}$ , **1**, and (b) a 0.28 mM solution of **5** in ACN under a N<sub>2</sub> atmosphere releases CO<sub>2</sub>(g) to generate  $[\text{Cu}_2(\mu\text{-OH})_2(\text{Me2m})]^{2+}$ , **2**.

nonbridging, controls the formation mechanism of the resulting carbonate complexes.

**Reversible CO<sub>2</sub> Fixation and Self-Assembly.** Carbon dioxide fixation by **1** and **2** is reversible, and purging the reaction mixture containing **4** and **5** with N<sub>2</sub>, respectively, leads to recovery of **1** and **2** (Figure 7). Exposure to a CO<sub>2</sub> atmosphere results in subsequent restoration of **4** and **5**. Such a cycle could be repeated several times without any apparent decomposition of the species involved. To further substantiate these observations, CO<sub>2</sub> release in CH<sub>3</sub>CN/water mixtures was performed for **4** and **6** at synthetic scale, under the same

conditions employed in the UV-vis measurements. **1** and **2** were isolated in 73% and 90% yields, respectively, and FT-IR analysis of the products lacks indication of carbonate features (Figure S16), suggesting that CO<sub>2</sub> release is quantitative. These experiments demonstrate that cage-like **4** can be reversibly assembled–disassembled by controlling the CO<sub>2</sub> concentration, without need of any kind of further chemical or electrochemical input. To the best of our knowledge, such ability has not been reported for copper complexes, although it has been described for Zn complexes that model carbonic anhydrase.<sup>46</sup> Interestingly, the rate of CO<sub>2</sub> release from **4** and **5** increases linearly with the water concentration (see Figures S17 and S18). The rate constant for CO<sub>2</sub> release ( $k_{\text{rel}}$ ) at  $[\text{H}_2\text{O}] = 1$  M is  $12.8 \times 10^{-3} \text{ M}^{-1} \text{ s}^{-1}$  for **4** and  $0.52 \times 10^{-3} \text{ M}^{-1} \text{ s}^{-1}$  for **5**. This trend is in agreement with the bond distances shown in Scheme 3, from which it follows that carbonate is more effectively bound in **5** than in **4**, and will therefore be released significantly slower. The overall analysis indicates that in spite of its enhanced nucleophilic reactivity, **1** could be isolated from CH<sub>3</sub>CN/H<sub>2</sub>O mixtures because of the significant hydrolytic sensitivity exhibited by **4**, a factor that could be traced to the particular binding mode of the carbonate ligand. In this sense, Parkin et al. have proposed that the coordination mode of the carbonate ligand determines its hydrolytic decomposition into hydroxide complexes and CO<sub>2</sub> release. In their analysis of different carbonate-bridged first-row transition metal complexes, the *anti-anti-μ-η<sup>1</sup>:η<sup>1</sup>* binding mode is especially prone to hydrolysis.<sup>46</sup>

CO<sub>2</sub> release from tetranuclear **8** does not occur under analogous conditions to **6**, and thus, the carbonate species appear to be somewhat more stable, presumably because of the chelate mode adopted by the carbonate ligand. However, addition of 1 equiv of HClO<sub>4</sub> per Cu atom to **8** does indeed cause CO<sub>2</sub> release and formation of dinuclear species **3**, as can be followed by UV-vis spectroscopy (Figure S19). Further addition of 1 equiv of Et<sub>3</sub>N per Cu atom restores **7**,

(46) Looney, A.; Han, R.; McNeill, K.; Parkin, G. *J. Am. Chem. Soc.* **1993**, *115*, 4690–4697.

which under a CO<sub>2</sub> atmosphere undergoes its fixation to regenerate **8**. Therefore, reversible self-assembly–disassembly of **8** could be accomplished by simple acid–base chemistry combined with CO<sub>2</sub> fixation. Although CO<sub>2</sub> is increasingly finding use in supramolecular chemistry by its reversible acid–base chemistry,<sup>47</sup> the strategy explored in this work has to the best of our knowledge no precedent in the literature.

On the basis of the kinetic data determined for the binding of CO<sub>2</sub>, it was concluded that HCO<sub>3</sub><sup>−</sup> is the species responsible for the formation of the carbonate complexes via a ligand substitution process. Low concentrations of water will cause dissolved CO<sub>2</sub> to undergo hydration to form HCO<sub>3</sub><sup>−</sup> which can also account for the formation of such complexes in organic solvents. The fact that kinetic complications were observed in mixed solvents can be accounted for in terms of the limited formation of HCO<sub>3</sub><sup>−</sup> under such conditions. On the other hand, excellent kinetic behavior was observed when HCO<sub>3</sub><sup>−</sup> was used directly to form the carbonate complexes. On the basis of microscopic reversibility, the reversible release of CO<sub>2</sub> by the carbonate complexes must also proceed via the formation of HCO<sub>3</sub><sup>−</sup> in solution that can undergo dehydration to release CO<sub>2</sub>(g).

## Conclusions

In this work we have studied the reaction between macrocyclic dicopper hydroxide complexes with CO<sub>2</sub>/HCO<sub>3</sub><sup>−</sup>, giving rise to a structurally diverse family of bridging carbonate species. Depending on the macrocyclic

ligand employed, CO<sub>2</sub> fixation can occur intra- or intermolecularly; in the former, the CO<sub>3</sub><sup>2−</sup> entity is buried within the hydrophobic macrocyclic cavity. In the latter, tetranuclear cagelike structures are assembled.

Kinetic studies demonstrate that fixation of CO<sub>2</sub> in these complexes can either occur via direct addition of CO<sub>2</sub> to the hydroxy ligand or via reaction of the hydroxy complex with HCO<sub>3</sub><sup>−</sup>, generated via hydration of CO<sub>2</sub>, in a ligand substitution process. The latter process seems to be extremely effective in terms of the reported kinetic data. This is an unexpected complication that should be seriously considered to understand CO<sub>2</sub> fixation reactions by transition metal complexes in the presence of water even in trace quantities, since this could be the only or major reaction route.

On the other hand, this work has resulted in two other promising findings. First, the reversible CO<sub>2</sub> binding by complex **2** to form **5**, which could be exclusively controlled by the [CO<sub>2</sub>] without the need of any external chemical, holds potential use as a CO<sub>2</sub> carrier. Second, this work demonstrates that small molecule activation (CO<sub>2</sub>) could be used to reversibly self-assemble supramolecular capsules, with potential applications in molecular recognition.

**Acknowledgment.** This research has been financed through projects CTQ2006-05367/BQU, CSD2006-0003 and CTQ2006-15634 (MEC, Spain), and the Deutsche Forschungsgemeinschaft within SFB 583 (Germany). A.C. and L.G. are grateful to MEC for FPU pre-doctoral grants.

**Supporting Information Available:** Crystallographic information files (CIF) for **3**, **4**, **5**, **6**, and **8**, structural details of **3**, and additional spectral, kinetic, and magnetic data. This material is available free of charge via the Internet at <http://pubs.acs.org>.

IC700692T

- (47) Rudkevich, D. M.; Xu, H. *Chem. Commun.* **2005**, *21*, 2651–2659.  
 (48) Youngme, S.; Chaichit, N.; Kongsaree, P.; van Albada, G. A.; Reedijk, J. *Inorg. Chim. Acta* **2001**, *324*, 232–240.  
 (49) Kruger, P. E.; Fallon, G. D.; Moubaraki, B.; Berry, K. J.; Murray, K. S. *Inorg. Chem.* **1995**, *34*, 4808–4814.  
 (50) Sletten, J.; Hope, H.; Julve, M.; Kahn, O.; Verdager, M.; Dworkin, A. *Inorg. Chem.* **1988**, *27*, 542–549.